Asymptotics of the Principal Eigenvalue of the Laplacian in 2-D Periodic Domains with Small Traps

F. Paquin-Lefebvre* , S. Iyaniwura † , M. J. Ward‡

May 1, 2021

Abstract

We derive and numerically implement various asymptotic approximations for the lowest or principal eigenvalue of the Laplacian with a periodic arrangement of localized traps of small $\mathcal{O}(\varepsilon)$ spatial extent that are centered at the lattice points of an arbitrary Bravais lattice in $\mathbb{R}^2$. The expansion of this principal eigenvalue proceeds in powers of $\nu \equiv -1/\log(\varepsilon d_c)$, where d_c is the logarithmic capacitance of the trap set. An explicit three-term approximation for this principal eigenvalue is derived using strong localized perturbation theory, with the coefficients in this series evaluated numerically by using an explicit formula for the source-neutral periodic Green's function and its regular part. Moreover, a transcendental equation for an improved approximation to the principal eigenvalue, which effectively sums all the logarithmic terms in powers of ν, is derived in terms of the regular part of the periodic Helmholtz Green's function. By using an Ewald summation technique to first obtain a rapidly converging infinite series representation for this regular part, a simple Newton iteration scheme on the transcendental equation is implemented to numerically evaluate the improved "log-summed" approximation to the principal eigenvalue. From a numerical computation of the PDE eigenvalue problem defined on the fundamental Wigner-Seitz cell for the lattice, it is shown that the three-term asymptotic approximation for the principal eigenvalue agrees well with the numerical result only for a rather small trap radius. In contrast, the log-summed asymptotic result provides a very close approximation to the principal eigenvalue even when the trap radius is only moderately small. For a circular trap, the first few transcendental correction terms that further improves the log-summed approximation for the principal eigenvalue are derived. Finally, it is shown numerically that, among all Bravais lattices with a fixed area of the primitive cell, the principal eigenvalue is maximized for a regular hexagonal arrangement of traps.

Key words: eigenvalue, Bravais lattice, logarithmic capacitance, periodic Green's function, trap cluster.

1 Introduction

For many elliptic and biharmonic problems in two spatial dimensions (2-D) with localized defects, such as perforations or obstacles, it is often challenging to provide accurate approximate solutions in the singularly perturbed limit $\varepsilon \to 0$ of a small defect size. Examples of such problems include eigenvalue problems for the Laplacian or Biharmonic operator in 2-D domains with small holes (cf. [24], [34], [17], [20], [18]), the calculation of the maximum voltage drop on a 2-D lattice of small circular power pads (cf. [1], [4]), the study of Faraday screening of electromagentic waves due to a wire mesh (cf. [5]), the determination of the mean first passage time for Brownian motion in 2-D domains with small traps (cf. [30], [26], [19], [32], [21], [3], [15]), and the analysis of Bloch waves in acoustics and electromagnetics for a 2-D lattice of small circular Dirichlet scatterers (cf. [29]), among others.

*Dept. of Mathematics, UBC, Vancouver, Canada. paquinl@math.ubc.ca
†Dept. of Mathematics, UBC, Vancouver, Canada. iyaniwura@math.ubc.ca
‡Dept. of Mathematics, UBC, Vancouver, Canada. (corresponding author ward@math.ubc.ca)

The primary difficulty with analyzing the effect of localized defects for many of these problems arises from the logarithmic singularity of the 2-D free-space Green's function. This weak singularity, as opposed to the stronger $1/r$ type singularity in 3-D, typically leads to an asymptotic expansion of the solution in powers of the logarithmic gauge $\nu = \mathcal{O}(-1/\log \varepsilon)$ when the defect has a Dirichlet condition imposed on its boundary. Owing to the slow convergence, unless ε is extremely small, of approximate solutions that involve a series in powers of this logarithmic gauge, in order to obtain an approximate solution with good accuracy one must either calculate many terms in this series or, preferably, sum the entire infinite logarithmic series. In contrast, for the $3-D$ case, the effect of the defect is typically $\mathcal{O}(\varepsilon)$ when a Dirichlet condition is imposed on its boundary.

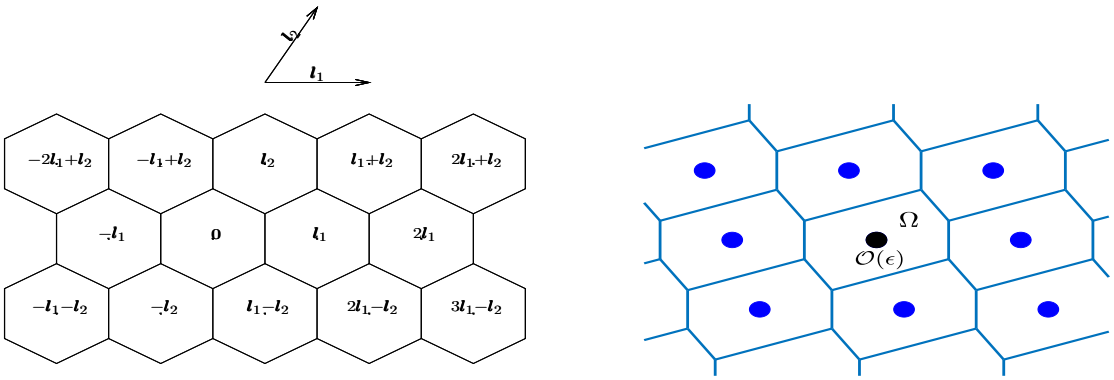

Figure 1: Left figure: part of an infinite regular hexagonal lattice showing the lattice vectors. The traps are centered at the lattice points. Right panel: Wigner Seitz (WS), or Voronoi, cells for an oblique Bravais lattice of circular traps (blue dots) of a common radius ε. The fundamental WS (FWS) cell Ω of unit area is centered at the origin and contains the black trap. The lattice vectors are $\boldsymbol{l}_1 = (1/\sqrt{\sin(\theta)}, 0)^T$ and $\boldsymbol{l}_2 = (\cos(\theta)/\sqrt{\sin(\theta)}, \sqrt{\sin(\theta)})^T$ with $\theta = \pi/5$. The circular traps can be replaced by a trap cluster of measure $\mathcal{O}(\varepsilon)$.

In this broad context, the specific goal of this paper is to derive and implement various asymptotic approximations for the lowest or principal eigenvalue of the Laplacian with a periodic arrangement of localized traps centered at the lattice points of an arbitrary Bravais lattice in $\mathbb{R}^2$. This principal eigenvalue provides an estimate for the rate at which a Brownian particle released from some location will become absorbed by one of the periodically arranged traps, with the reciprocal of the principal eigenvalue providing an approximation for the mean first capture time. The characterization of the mean first passage time for diffusion in heterogeneous media where a diffusing particle can become absorbed by localized traps arises in various applications such as heterogeneous catalysis and nutrient uptake in cells (see [30], [7], [16], [10] and the references therein).

The implementation of our singular perturbation analysis to approximate the principal eigenvalue will rely heavily on explicit analytical formulae for certain Green's functions with singularities at the lattice points. More specifically, we consider a spatially periodic array of traps in $\mathbb{R}^2$ where either a single trap or a trap cluster of small $\mathcal{O}(\varepsilon)$ measure is centered at the lattice points of an oblique Bravais lattice Λ defined by

$$\Lambda \equiv \left\{ m\boldsymbol{l}_1 + n\boldsymbol{l}_2 \,\middle|\, m,\, n \in \mathbb{Z} \right\}, \tag{1.1}$$

where $\mathbb{Z}$ denotes the set of integers. The *Wigner-Seitz (WS)* cell centered at a fixed $\boldsymbol{l} \in \Lambda$ is the set of all points in

the plane that are closer to $\boldsymbol{l}$ than to any other lattice point. The fundamental Wigner-Seitz (FWS) cell Ω is the one centered at the origin (see the right panel of Fig. 1 with the black trap). A WS cell is a convex polygon that has the same area $|\boldsymbol{l}_1 \times \boldsymbol{l}_2|$ of the primitive cell, and the union of these WS cells tile all of $\mathbb{R}^2$. We will choose the lengthscale so that the area of the primitive cell is fixed at unity. For a particular oblique lattice, in the right panel of Fig. 1 we show the WS cells with a single circular trap (blue disk) of radius ε centered at each lattice point, and the FWS cell Ω centered at the origin (black disk). In the left panel of Fig. 1 we show the lattice vectors for a hexagonal lattice.

In the limit $\varepsilon \to 0$ of small trap measure we will calculate the principal eigenvalue of the Laplacian where a common trap cluster is centered at the lattice points of (1.1). This problem can be reduced to an eigenvalue problem on the FWS cell Ω of unit area, and is formulated as

$$\triangle \Phi + \lambda \Phi = 0\,, \quad \boldsymbol{x} \in \Omega \backslash \Omega_\varepsilon\,; \qquad \Phi \in \mathcal{P}\,, \quad \boldsymbol{x} \in \partial\Omega\,, \tag{1.2a}$$

$$\Phi = 0\,, \quad \boldsymbol{x} \in \partial\Omega_\varepsilon\,; \qquad \int_{\Omega\backslash\Omega_\varepsilon} \Phi^2 \, d\boldsymbol{x} = 1\,. \tag{1.2b}$$

Here Ω_ε denotes a possibly multiply connected trap cluster of measure $\mathcal{O}(\varepsilon)$ centered at the origin $\mathbf{0} \in \Omega$. In (1.2a) the operator $\mathcal{P}$ denotes periodic boundary conditions on $\partial\Omega$ (see (A.7) of Appendix A for a precise formulation).

The challenge in providing a good approximation for the principal eigenvalue of (1.2), even when the trap size ε is only moderately small, is that the term-by-term asymptotic expansion of this eigenvalue proceeds in powers of $\nu \equiv -1/\log(\varepsilon d_c)$, where d_c is the logarithmic capacitance of the the trap set.

By exploiting the analytical result of [6] for the periodic source-neutral Green's function and its regular part, in Principal Result 1 of §2 a new explicit three-term expansion in powers of ν for the principal eigenvalue of (1.2) is derived. The third term in this expansion is shown to depend on an integral of this periodic Green's function over the FWS cell of the lattice. From a numerical quadrature of this term, we show that the principal eigenvalue is maximized, over the class of Bravais lattices, for a regular hexagonal lattice. In §3 we formulate a transcendental equation that provides an improved approximation to this principal eigenvalue, and which is defined in terms of the regular part of a periodic Helmholtz Green's function. This "log-summed" approximation effectively sums all of the logarithmic corrections in powers of ν in the asymptotic approximation for the principal eigenvalue of (1.2). By extending the methodology of [2], in Principal Result 2 of §3 we derive a new computationally tractable representation for the regular part of the Helmholtz Green's function, which involves two rapidly converging lattice sums. In this way, in §3.1 we provide numerical results, based on a simple Newton iteration scheme applied to the transcendental equation (3.7), for the log-summed approximation to the principal eigenvalue of (1.2) for an arbitrary Bravais lattice. For the case of a circular trap of radius ε, in Principal Result 3 of §4 a more refined approximation to the principal eigenvalue is obtained, which is based on calculating the first few transcendentally small terms in its asymptotic expansion that are smaller than any power of ν.

In §4.1, we compare our various asymptotic approximations for the principal eigenvalue with corresponding full numerical results for (1.2) that are computed from FlexPDE [9] for both a square and a regular hexagonal lattice. These comparisons show that, although the three-term approximation in Principal Result 1 provides a decent approximation to the principal eigenvalue when ε is rather small, the log-summed approximation based on a Newton iteration scheme applied to (3.7) provides a much closer approximation when ε is only moderately small. For a square lattice with a circular trap at each lattice point, our three-term asymptotic result for the principal eigenvalue of (1.2) is shown to

agree with that derived previously in [30] using a pseudo-potential approximation combined with a numerical evaluation of certain discrete lattice sums.

We emphasize that the transcendental equation (3.7) and its numerical implementation applies not just for a circular trap, but also for an arbitrarily-shaped trap or for a cluster of traps, as characterized by the logarithmic capacitance d_c of the trap set. For a trap cluster consisting of a collection of non-overlapping circular disks, in §4.2 we show how to numerically compute d_c to a high degree of accuracy by using a series-based approach inspired by the methodology in [31] (see also [14]). This approach is illustrated for a two-disk cluster, where an analytical solution is available for comparison, as well as for a three-disk cluster. Finally, a brief discussion is given in §5.

2 Asymptotics of the principal eigenvalue

The term-by-term asymptotic analysis for the principal eigenvalue of (1.2) as $\varepsilon \to 0$ relies on the periodic source-neutral Green's function $G_p(\boldsymbol{x})$ with regular part R_p, defined uniquely by

$$\Delta G_p = \frac{1}{|\Omega|} - \delta(\boldsymbol{x})\,, \quad \boldsymbol{x} \in \Omega\,; \quad G_p \in \mathcal{P}\,, \quad \boldsymbol{x} \in \partial\Omega\,; \quad \int_\Omega G_p\, d\boldsymbol{x} = 0\,, \tag{2.1a}$$

$$G_p = -\frac{1}{2\pi}\log|\boldsymbol{x}| + R_p + \frac{|\boldsymbol{x}|^2}{4} + o(|\boldsymbol{x}|^2)\,, \quad \text{as} \quad \boldsymbol{x} \to \boldsymbol{0}\,. \tag{2.1b}$$

Since Ω has two lines of symmetry that intersect at the origin, the usual gradient term $\nabla_{\boldsymbol{x}} G_p|_{\boldsymbol{x}=\boldsymbol{0}} \cdot \boldsymbol{x}$ is absent in the local behavior (2.1b).

In [6] an explicit formula for $G_p(\boldsymbol{x})$ and R_p was derived in their analysis of droplet patterns in diblock copolymer theory. In their analysis, a point $\boldsymbol{x}$ is represented as a complex number $z = x + iy$ and the Bravais lattice was written equivalently in terms of generators $\alpha \in \mathbb{C}$ and $\beta \in \mathbb{C}$ as $\Lambda \equiv \left\{ m\alpha + n\beta \,\middle|\, m,\, n \in \mathbb{Z} \right\}$. By setting $\mathrm{Im}(\beta/\alpha) > 0$ and $\mathrm{Im}(\bar{\alpha}\beta) = 1$, the area of primitive cell was fixed to unity. In terms of these generators, it was derived in [6] that

$$\begin{aligned} G_p(z) = {} & \mathrm{Im}\left(\frac{|z|^2 - \bar{\alpha} z^2/\alpha}{2(\alpha\bar{\beta} - \bar{\alpha}\beta)} - \frac{z}{2\alpha} + \frac{\beta}{12\alpha} \right) \\ & - \frac{1}{2\pi}\log\left| \left(1 - e\left(\frac{z}{\alpha}\right)\right) \times \prod_{n=1}^{\infty} \left(1 - e\left(\frac{n\beta + z}{\alpha}\right)\right)\left(1 - e\left(\frac{n\beta - z}{\alpha}\right)\right) \right|, \end{aligned} \tag{2.2a}$$

where $e(w) \equiv e^{2\pi i w}$. Here the overbar denotes complex conjugate. In terms of $\zeta \equiv \beta/\alpha$, the regular part R_p of G_p is

$$R_p = -\frac{1}{2\pi}\log(2\pi) - \frac{1}{2\pi}\log\left| \sqrt{\mathrm{Im}(\zeta)}\, e\left(\frac{\zeta}{12}\right) \prod_{n=1}^{\infty} (1 - e(n\zeta))^2 \right|. \tag{2.2b}$$

Our three-term asymptotic result for the principal eigenvalue of (1.2), defined in terms of G_p and R_p, is as follows:

Principal Result 1 *For $\varepsilon \to 0$, the principal eigenvalue λ_0 for (1.2) for an arbitrary oblique Bravais lattice is*

$$\lambda_0 = \nu\lambda_{00} + \nu^2\lambda_{01} + \nu^3\lambda_{02} + \mathcal{O}(\nu^4)\,, \tag{2.3a}$$

where the coefficients are given in terms of R_p and G_p in (2.2) by

$$\lambda_{00} = 2\pi\,, \qquad \lambda_{01} = -4\pi^2 R_p\,, \qquad \lambda_{02} = 8\pi^3\left[R_p^2 - \int_\Omega G_p^2\, d\boldsymbol{x} \right]. \tag{2.3b}$$

In (2.3a), $\nu = -1/\log(\varepsilon d_c)$, where d_c is the logarithmic capacitance of the re-scaled trap cluster $\Omega_0 \equiv \varepsilon^{-1}\Omega_\varepsilon$, which is defined in terms of the local coordinate $\boldsymbol{y} = \varepsilon^{-1}\boldsymbol{x}$ by the canonical inner problem

$$\begin{aligned} &\Delta_{\boldsymbol{y}} v_c = 0\,, \quad \boldsymbol{y} \notin \Omega_0\,; \quad v_c = 0\,, \quad \boldsymbol{y} \in \partial\Omega_0\,, \\ &\quad v_c \sim \log|\boldsymbol{y}| - \log d_c + \frac{\boldsymbol{p}_c\cdot\boldsymbol{y}}{|\boldsymbol{y}|^2} + \cdots\,, \quad \text{as} \quad |\boldsymbol{y}| \to \infty\,. \end{aligned} \tag{2.4}$$

To derive (2.3) we use the framework of strong localized perturbation theory for 2-D singular perturbation problems, as introduced in [34] and [35]. This methodology, based on the method of matched asymptotic expansions, is tailored for PDE problems with localized defects. The effect of the defect structure in the far-field typically involves either monopole or dipole termss, which are conveniently encapsulated by including various Dirac source functions in the outer solution. A survey of this approach to a broad range of diffusive problems is given in [33].

In the outer region, defined for $|\boldsymbol{x}| \gg \mathcal{O}(\varepsilon)$, we substitute the eigenvalue expansion (2.3a), together with the outer expansion

$$\Phi = \Phi_0 + \nu\Phi_1 + \nu^2\Phi_2 + \nu^3\Phi_3 + \cdots\,, \tag{2.5}$$

into (1.2), and then collect powers of ν. At leading order we get $\Delta\Phi_0 = 0$ in Ω with $\Phi_0 \in \mathcal{P}$ on $\partial\Omega$ and $\int_\Omega \Phi_0^2\,d\boldsymbol{x} = 1$, so that $\Phi_0 = 1$. At order $\mathcal{O}(\nu^k)$ for $k = 1, 2, 3$, we obtain, respectively, that

$$\Delta\Phi_1 = -\lambda_{00}\Phi_0\,, \quad \boldsymbol{x} \in \Omega\backslash\{\boldsymbol{0}\}\,; \qquad \Phi_1 \in \mathcal{P}\,, \quad \boldsymbol{x} \in \partial\Omega\,, \tag{2.6a}$$

$$\Delta\Phi_2 = -\lambda_{00}\Phi_1 - \lambda_{01}\Phi_0\,, \quad \boldsymbol{x} \in \Omega\backslash\{\boldsymbol{0}\}\,; \qquad \Phi_2 \in \mathcal{P}\,, \quad \boldsymbol{x} \in \partial\Omega\,, \tag{2.6b}$$

$$\Delta\Phi_3 = -\lambda_{00}\Phi_2 - \lambda_{01}\Phi_1 - \lambda_{02}\Phi_0\,, \quad \boldsymbol{x} \in \Omega\backslash\{\boldsymbol{0}\}\,; \qquad \Phi_3 \in \mathcal{P}\,, \quad \boldsymbol{x} \in \partial\Omega\,, \tag{2.6c}$$

which are subject to the normalization conditions

$$\int_\Omega \Phi_0\Phi_1\,d\boldsymbol{x} = 0\,, \qquad \int_\Omega \Phi_0\Phi_2\,d\boldsymbol{x} = -\frac{1}{2}\int_\Omega \Phi_1^2\,d\boldsymbol{x}\,, \qquad \int_\Omega \Phi_0\Phi_3\,d\boldsymbol{x} = -\int_\Omega \Phi_1\Phi_2\,d\boldsymbol{x}\,. \tag{2.6d}$$

In the inner region near the trap cluster Ω_ε centered at $\boldsymbol{x} = \boldsymbol{0}$ we introduce the inner variables

$$\boldsymbol{y} = \varepsilon^{-1}\boldsymbol{x}\,, \qquad v(\boldsymbol{y}) \equiv \Phi(\varepsilon\boldsymbol{y})\,. \tag{2.7}$$

We then expand the inner solution in terms of undetermined coefficients A_i for $i \geq 1$, which are independent of ν, as

$$v(\boldsymbol{y}) = \left(\nu + A_1\nu^2 + A_2\nu^3 + A_3\nu^4 + \cdots\right) v_c(\boldsymbol{y}) + \mathcal{O}(\sigma(\varepsilon))\,, \tag{2.8}$$

where $\sigma(\varepsilon) \ll \nu^k$ for any $k > 1$. Here $\nu \equiv -1/\log(\varepsilon d_c)$ and v_c satisfies the canonical inner problem (2.4), which defines the logarithmic capacitance d_c of the trap cluster. We will show below in §4 that the transcendentally small term σ in (2.8) is in fact $\sigma = \mathcal{O}(\varepsilon^2)$. Upon using the far-field behavior of v_c in (2.8), and writing the resulting expression in outer variables, we obtain that the outer solution must satisfy the following singularity behavior up to $\mathcal{O}(\nu^3)$ terms:

$$\Phi = 1 + \nu\left(\log|\boldsymbol{x}| + A_1\right) + \nu^2\left(A_1\log|\boldsymbol{x}| + A_2\right) + \nu^3\left(A_2\log|\boldsymbol{x}| + A_3\right) + \cdots\,, \quad \text{as} \quad \boldsymbol{x} \to \boldsymbol{0}\,. \tag{2.9}$$

Upon comparing (2.9) with (2.5) at each order in ν, we conclude that the problems in (2.6) must satisfy the following singularity conditions as $\boldsymbol{x} \to \boldsymbol{0}$:

$$\Phi_1 \sim \log|\boldsymbol{x}| + A_1\,; \qquad \Phi_2 \sim A_1\log|\boldsymbol{x}| + A_2\,; \qquad \Phi_3 \sim A_2\log|\boldsymbol{x}| + A_3\,. \tag{2.10}$$

From (2.6a) and (2.10), the problem for Φ_1, with $\Phi_0 \equiv 1$, can be written in terms of the Dirac distribution as

$$\begin{aligned} &\Delta\Phi_1 = -\lambda_{00} + 2\pi\delta(\boldsymbol{x})\,, \quad \boldsymbol{x}\in\Omega\,; \qquad \Phi_1\in\mathcal{P}\,, \quad \boldsymbol{x}\in\partial\Omega\,, \\ &A_1 = \lim_{\boldsymbol{x}\to\boldsymbol{0}}\left(\Phi_1 - \log|\boldsymbol{x}|\right)\,; \qquad \int_\Omega \Phi_1\,d\boldsymbol{x} = 0\,. \end{aligned} \tag{2.11}$$

By using the divergence theorem, together with the periodic boundary conditions and $|\Omega| = 1$, we deduce that $\lambda_{00} = 2\pi$. Then, by comparing (2.11) with (2.1), we identify that

$$\Phi_1 = -2\pi G_p(\boldsymbol{x})\,, \qquad A_1 = -2\pi R_p\,, \tag{2.12}$$

where G_p is the periodic source-neutral Green's function with regular part R_p, as given explicitly in (2.2).

At order $\mathcal{O}(\nu^2)$, we obtain from (2.6b) and (2.10) that Φ_2 satisfies

$$\begin{aligned} &\Delta\Phi_2 = -\lambda_{00}\Phi_1 - \lambda_{01} + 2\pi A_1\delta(\boldsymbol{x})\,, \quad \boldsymbol{x}\in\Omega\,; \qquad \Phi_2\in\mathcal{P}\,, \quad \boldsymbol{x}\in\partial\Omega\,, \\ &A_2 = \lim_{\boldsymbol{x}\to\boldsymbol{0}}\left(\Phi_2 - A_1\log|\boldsymbol{x}|\right)\,; \qquad \int_\Omega \Phi_2\,d\boldsymbol{x} = -\frac{1}{2}\int_\Omega \Phi_1^2 d\boldsymbol{x}\,. \end{aligned} \tag{2.13}$$

By using the divergence theorem together with the periodic boundary conditions we get that

$$-\lambda_{00}\int_\Omega \Phi_1\,d\boldsymbol{x} - \lambda_{01}|\Omega| + 2\pi A_1 = 0\,.$$

Since $|\Omega| = 1$ and $\int_\Omega \Phi_1\,d\boldsymbol{x} = 0$, we conclude that

$$\lambda_{01} = 2\pi A_1\,, \quad \text{where} \quad A_1 = -2\pi R_p\,. \tag{2.14}$$

Next, we decompose the solution to (2.13) as

$$\Phi_2 = -2\pi A_1 G_p(\boldsymbol{x}) + 2\pi\lambda_{00}\Phi_{2p}(\boldsymbol{x}) = 4\pi^2 R_p G_p(\boldsymbol{x}) + 4\pi^2\Phi_{2p}(\boldsymbol{x})\,. \tag{2.15}$$

Upon substituting (2.15) into (2.13), and using (2.12) for Φ_1, we obtain after some algebra that Φ_{2p} satisfies

$$\begin{aligned} &\Delta\Phi_{2p} = G_p(\boldsymbol{x})\,, \quad \boldsymbol{x}\in\Omega\,; \qquad \Phi_{2p}\in\mathcal{P}\,, \quad \boldsymbol{x}\in\partial\Omega\,; \qquad \int_\Omega \Phi_{2p}\,d\boldsymbol{x} = -\frac{1}{2}\int_\Omega G_p^2\,d\boldsymbol{x}\,, \\ &A_2 = 4\pi^2\lim_{\boldsymbol{x}\to\boldsymbol{0}}\Phi_{2p}(\boldsymbol{x}) + 4\pi^2 R_p\lim_{\boldsymbol{x}\to\boldsymbol{0}}\left(G_p(\boldsymbol{x}) + \frac{1}{2\pi}\log|\boldsymbol{x}|\right)\,. \end{aligned} \tag{2.16}$$

Since Φ_{2p} is bounded as $\boldsymbol{x}\to 0$, we calculate by using the local behavior for G_p in (2.1b) that

$$A_2 = 4\pi^2\left[R_p^2 + \Phi_{2p}(\boldsymbol{0})\right]\,. \tag{2.17}$$

Next, at order $\mathcal{O}(\nu^3)$, we obtain from (2.6) and (2.10) that Φ_3 satisfies

$$\Delta\Phi_3 = -\lambda_{00}\Phi_2 - \lambda_{01}\Phi_1 - \lambda_{02} + 2\pi A_2\delta(\boldsymbol{x})\,, \quad \boldsymbol{x}\in\Omega\,; \qquad \Phi_3\in\mathcal{P}\,, \quad \boldsymbol{x}\in\partial\Omega\,. \tag{2.18}$$

From the divergence theorem and the periodic boundary conditions, and by using $|\Omega| = 1$ and $\int_\Omega \Phi_1\,d\boldsymbol{x} = 0$, we calculate λ_{02} as

$$\lambda_{02} = 2\pi A_2 - \lambda_{00}\int_\Omega \Phi_2\,d\boldsymbol{x}\,, \qquad \text{where} \quad \int_\Omega \Phi_{2p}\,d\boldsymbol{x} = -\frac{1}{2}\int_\Omega \Phi_1^2\,d\boldsymbol{x}\,. \tag{2.19}$$

Then, upon using $\lambda_{00} = 2\pi$, and $\Phi_1 = -2\pi G_p(\boldsymbol{x})$, we obtain

$$\lambda_{02} = 8\pi^3 \left(R_p^2 + \Phi_{2p}(\mathbf{0}) + \frac{1}{2} \int_\Omega \left[G_p(\boldsymbol{x}) \right]^2 \, d\boldsymbol{x} \right) , \tag{2.20}$$

where $\Phi_{2p}(\mathbf{0})$ is to be calculated from the PDE (2.16).

Finally, we show that $\Phi_{2p}(\mathbf{0})$ can be evaluated without having to solve the PDE (2.16). By using Green's second identity on (2.16) and (2.1), we obtain from the periodic boundary conditions that $\int_\Omega G_p \Delta \Phi_{2p} \, d\boldsymbol{x} = \int_\Omega \Phi_{2p} \Delta G_p \, d\boldsymbol{x}$. Since $|\Omega| = 1$, this yields that $\int_\Omega G_p^2 \, d\boldsymbol{x} = -\Phi_{2p}(\mathbf{0}) + \int_\Omega \Phi_{2p} \, d\boldsymbol{x}$. By using (2.16) for $\int_\Omega \Phi_{2p} \, d\boldsymbol{x}$, this yields that $\Phi_{2p}(\mathbf{0}) = -(3/2) \int_\Omega [G_p]^2 \, d\boldsymbol{x}$. By substituting this expression into (2.20), we obtain the result for λ_{02}, as given in (2.3b). This complete the derivation of Principal Result 1.

The three-term asymptotic expansion (2.3) for the principal eigenvalue λ_0 of (1.2) depends only on the periodic source-neutral Green's function and its regular part, as given explicitly in (2.2). The integral $\int_\Omega G_p^2 \, d\boldsymbol{x}$ in the second order coefficient λ_{20} can be calculated numerically from the routine *intpoly* in MATLAB [22]. This routine is ideally suited for performing a quadrature over the polygonal-shaped FWS cell.

For a Bravais lattice with unit area of the primitive cell, it was proved in Theorem 2 of [6] that R_p in (2.2b) is minimized for a regular hexagonal lattice. As such, within this comparison group, we conclude that the leading order eigenvalue correction λ_{01} in (2.3) is maximized for a hexagonal lattice.

We will illustrate (2.3) for the one-parameter family of lattices Λ with generators

$$\boldsymbol{l}_1 = (1/\sqrt{\sin(\theta)}, 0)^T , \qquad \boldsymbol{l}_2 = (\cos(\theta)/\sqrt{\sin(\theta)}, \sqrt{\sin(\theta)})^T \tag{2.21}$$

For this class we have $|\boldsymbol{l}_1| = |\boldsymbol{l}_2|$ and it corresponds to setting $\alpha = 1/\sqrt{\sin\theta}$ and $\beta = \alpha e^{i\theta}$ in (2.2b). This yields that

$$R_p = -\frac{1}{2\pi} \ln(2\pi) - \frac{1}{2\pi} \ln \left| \sqrt{\sin\theta} \, e^{\pi i \xi/6} \prod_{n=1}^{\infty} \left(1 - e^{2\pi i n \xi} \right)^2 \right| , \quad \xi = e^{i\theta} . \tag{2.22}$$

For a hexagonal and square lattice where $\theta = \pi/3$ and $\theta = \pi/2$, we calculate that $R_p \approx -0.210262$ and $R_p \approx -0.208578$, respectively.

In Fig. 2 we plot the numerically computed coefficients λ_{01} and λ_{02}, given in (2.3b), for oblique Bravais lattices with generators given in (2.21). As expected, λ_{01} is maximized for the hexagonal lattice where $\lambda_{01} = \pi/3$. As a check on the quadrature of $\int_\Omega G_p^2 \, d\boldsymbol{x}$ using *intpoly* in MATLAB [22], we equivalently performed the integration over the primitive cell $\Omega_0 \equiv \{ z \,|\, z = s\alpha + t\beta \,, \; 0 < s, t < 1 \}$ in that

$$\int_\Omega \left[G_p(z) \right]^2 d\boldsymbol{x} = \int_{\Omega_0} \left[G_p(z) \right]^2 \, d\boldsymbol{x} = \int_0^1 \int_0^1 \left[G_p(s\alpha + t\beta) \right]^2 \, \mathrm{Im}(\bar{\alpha}\beta) \, ds \, dt \, , \tag{2.23}$$

where $\mathrm{Im}(\bar{\alpha}\beta) = 1$. The integration in (2.23) over the square $0 \le s \le 1$ and $0 \le t \le 1$ was performed with a product of Gauss-Legendre rules with 255×255 subdivisions. Although, there are mild logarithmic singularities of G_p at each of the four corners of this square that affect the accuracy of the quadrature, as a check on the numerical procedure we verified that $| \int_{\Omega_0} G_p \, d\boldsymbol{x}| \le 10^{-10}$. In particular, for the hexagonal and square lattices we calculate that

$$\lambda_0 \sim 2\pi\nu + \begin{cases} (8.2343)\nu^2 + (9.8321)\nu^3 + \cdots , & \text{(square)} \\ (8.3008)\nu^2 + (10.0459)\nu^3 + \cdots , & \text{(hexagon)} \, . \end{cases} \tag{2.24}$$

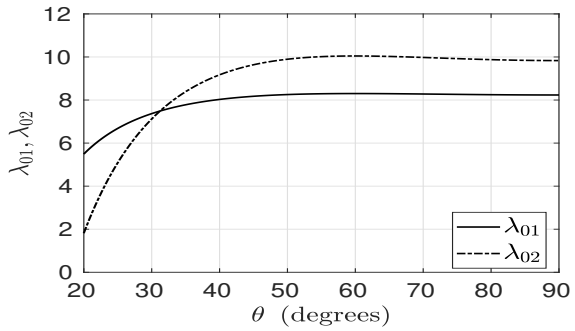

Figure 2: Plot of the coefficients λ_{01} and λ_{02} in the eigenvalue expansion (2.3) versus the angle θ (degrees) for an oblique Bravais lattice with generators $\boldsymbol{l}_1 = (1/\sqrt{\sin(\theta)}, 0)^T$ and $\boldsymbol{l}_2 = (\cos(\theta)/\sqrt{\sin(\theta)}, \sqrt{\sin(\theta)})^T$. The maximum of λ_{01} occurs for the hexagon $\theta = \pi/3$.

In [30] the method of pseudo-potentials combined with a separation of variables approach was used to derive a three-term expansion for the fundamental eigenvalue on a square or triangular lattice that contains a circular trap of radius ε centered at the lattice points. For a square lattice of unit area of the primitive cell, [30] obtained that

$$\lambda_0 = \lambda_{0t} \sim 2\pi\nu \left[1 + \alpha_s \nu + \left(\alpha_s^2 - \frac{\beta_s}{\pi^2} \right) \nu^2 + \cdots \right], \tag{2.25}$$

where $\alpha_s \approx 1.310529$ and $\beta_s \approx 1.506703$ were obtained from a numerical evaluation of certain discrete lattice sums. This result for the square lattice agrees with that in (2.24). Our three-term result (2.3) in Principal Result 1 extends this previous result to arbitrary 2-D Bravais lattices and to allow for non-circular trap geometries or a cluster of traps, as characterized by the logartihmic capacitance.

3 Summing the asymptotic expansion for the principal eigenvalue

In this section we derive a nonlinear transcendental equation that effectively sums the entire infinite logarithmic expansion for the principal eigenvalue λ_0 of (1.2). To do so we write the inner solution (2.8) as

$$\boldsymbol{y} = \varepsilon^{-1}\boldsymbol{x}\,, \qquad v(\boldsymbol{y}) \equiv \Phi(\varepsilon \boldsymbol{y})\,, \tag{3.1}$$

where

$$v(\boldsymbol{y}) = A(\nu) v_c(\boldsymbol{y}) + \mathcal{O}(\sigma_i)\,, \qquad \nu \equiv -1/\log(\varepsilon d_c)\,, \tag{3.2}$$

and $\sigma_i \ll \nu^k$ for any $k \geq 1$. In addition, the eigenvalue and outer solution are expanded as

$$\lambda_0 = \lambda_{0s}(\nu) + \mathcal{O}(\sigma_0)\,; \qquad \Phi = \Phi_{0s}(\boldsymbol{x};\nu) + \mathcal{O}(\sigma_0)\,, \tag{3.3}$$

where $\sigma_0 \ll \nu^k$ for any $k \geq 1$. By using the far-field behavior of $v_c(\boldsymbol{y})$ from (2.4) in (3.2) to match to the outer solution we obtain that λ_{0s} and Φ_{0s} satisfy

$$\Delta\Phi_{0s} + \lambda_{0s}\Phi_{0s} = 0\,, \quad \boldsymbol{x} \in \Omega\backslash\{\boldsymbol{0}\}\,; \qquad \Phi_{0s} \in \mathcal{P}\,, \quad \boldsymbol{x} \in \partial\Omega\,, \tag{3.4a}$$

$$\Phi_{0s} = A \log|\boldsymbol{x}| + \frac{A}{\nu} + o(1)\,, \quad \text{as} \quad \boldsymbol{x} \to \boldsymbol{0}\,; \qquad \int_\Omega \Phi_{0s}^2 \, d\boldsymbol{x} = 1\,. \tag{3.4b}$$

Since the local behavior in (3.4b) specifies the regular part of the singularity condition, this constraint effectively determines an equation for λ_{0s}.

The solution to (3.4) that has the correct singularity as $\boldsymbol{x} \to 0$, and which satisfies $\int_\Omega \Phi_{0s}^2 \, d\boldsymbol{x} = 1$, is simply

$$\Phi_{0s} = -2\pi A G_\lambda(\boldsymbol{x}) \,, \qquad \text{where} \qquad A = \frac{1}{2\pi} \left[\int_\Omega \left[G_\lambda(\boldsymbol{x}) \right]^2 \, d\boldsymbol{x} \right]^{-1/2} \,, \tag{3.5}$$

where $G_\lambda(\boldsymbol{x})$ is the periodic Helmholtz Green's function, with regular part R_λ, defined on the FWS cell Ω by

$$\Delta G_\lambda + \lambda_{0s} G_\lambda = -\delta(\boldsymbol{x}) \,, \quad \boldsymbol{x} \in \Omega \,; \quad G_\lambda \in \mathcal{P} \,, \quad \boldsymbol{x} \in \partial\Omega \,, \tag{3.6a}$$

$$G_\lambda = -\frac{1}{2\pi} \log|\boldsymbol{x}| + R_\lambda + \mathcal{O}(|\boldsymbol{x}|^2 \log|\boldsymbol{x}|) \,, \quad \text{as} \quad \boldsymbol{x} \to \boldsymbol{0} \,. \tag{3.6b}$$

Once again, since Ω has two lines of symmetry that intersect at the origin, the usual gradient term $\nabla_{\boldsymbol{x}} G_\lambda|_{\boldsymbol{x}=\boldsymbol{0}} \cdot \boldsymbol{x}$ is absent in the local behavior (3.6b).

To derive the eigenvalue relation that will determine λ_{0s} we let $\boldsymbol{x} \to \boldsymbol{0}$ in (3.5) and equate the regular part of this expression with that in (3.4b), which yields $-2\pi A R_\lambda = A/\nu$. In this way, we obtain that λ_{0s} is given by the smallest positive root of the transcendental equation

$$R_\lambda = -\frac{1}{2\pi\nu} \,, \qquad \text{where} \quad \nu \equiv -\frac{1}{\log(\varepsilon d_c)} \,, \tag{3.7}$$

where R_λ depends on λ_{0s} from the solution to (3.6).

The key to numerically implementing a root-finding condition on (3.7) for $\lambda_{0s} = \lambda_{0s}(\nu)$ is to derive a computationally tractable explicit formula for R_λ that can be used for an arbitrary Bravais lattice. The challenge is that it is well-known that standard Fourier transform methods yield very slowly converging infinite series representations, which are not well-suited for computations. To derive an alternative rapidly converging representation for R_λ, in Appendix B we first summarize the methodology of [2], which is based on the Poisson summation formula. This approach of [2] yields the explicit result

$$G_\lambda(\boldsymbol{x}) = \sum_{\boldsymbol{d} \in \Lambda^\star} \frac{e^{-\left(4\pi^2|\boldsymbol{d}|^2 - \lambda_{0s}\right)/\eta^2}}{4\pi^2|\boldsymbol{d}|^2 - \lambda_{0s}} \, e^{2\pi i \boldsymbol{x}\cdot\boldsymbol{d}} + F_{\text{sing}}(|\boldsymbol{x}|) + \sum_{\substack{\boldsymbol{l} \in \Lambda \\ \boldsymbol{l} \neq \boldsymbol{0}}} F_{\text{sing}}(|\boldsymbol{x} + \boldsymbol{l}|) \,, \tag{3.8a}$$

valid for $\lambda_{0s} \neq 4\pi^2|\boldsymbol{d}|^2$ for any $\boldsymbol{d} \in \Lambda^\star$. Here $F_{\text{sing}}(r)$ is defined by

$$F_{\text{sing}}(r) \equiv \frac{1}{2\pi} \int_{\log\eta}^{\infty} e^{-\frac{r^2}{4} e^{2s} + \lambda_{0s} e^{-2s}} \, ds \,. \tag{3.8b}$$

In (3.8a), $\Lambda^\star$ is the dual lattice to Λ, which is defined in terms of reciprocal lattice vectors $\boldsymbol{d}_1$ and $\boldsymbol{d}_2$ by

$$\Lambda^\star = \left\{ m\boldsymbol{d}_1 + n\boldsymbol{d}_2 \,\middle|\, m, n \in \mathbb{Z} \right\} , \qquad \text{with} \quad \boldsymbol{d}_i \cdot \boldsymbol{l}_j = \delta_{ij} \,, \tag{3.9}$$

where δ_{ij} is the Kronecker symbol. In (3.8), $\eta > 0$ is a user-defined Ewald cut-off parameter that is chosen so that the infinite sums over the lattice and dual lattice both converge rapidly.

Next, we take the limit $\boldsymbol{x} \to \boldsymbol{0}$ in (3.8) so as to identify that R_λ in (3.6b) is given by

$$R_\lambda \equiv \lim_{\boldsymbol{x} \to \boldsymbol{0}} \left(G_\lambda(\boldsymbol{x}) + \frac{1}{2\pi} \log|\boldsymbol{x}| \right) . \tag{3.10}$$

As is evident from (3.8), the logarithmic singularity for $G_\lambda(\boldsymbol{x})$ as $\boldsymbol{x} \to \boldsymbol{0}$ arises from the $F_{\text{sing}}(|\boldsymbol{x}|)$ term in (3.8b), owing to the fact that the integrand defining $F_{\text{sing}}(0)$ is not integrable. Our result for R_λ is as follows:

Principal Result 2 *The regular part R_λ, as defined by (3.10), is given by*

$$R_\lambda = \sum_{\boldsymbol{d}\in\Lambda^\star} \frac{e^{-\left(4\pi^2|\boldsymbol{d}|^2-\lambda_{0s}\right)/\eta^2}}{4\pi^2|\boldsymbol{d}|^2-\lambda_{0s}} + F_{\rm reg} + \sum_{\substack{\boldsymbol{l}\in\Lambda\\ \boldsymbol{l}\neq\boldsymbol{0}}} F_{\rm sing}(|\boldsymbol{l}|)\,, \tag{3.11a}$$

which is valid for $\lambda_{0s} \neq 4\pi^2|\boldsymbol{d}|^2$ for any $\boldsymbol{d}\in\Lambda^\star$. Here $F_{\rm reg}$ is given explicitly by

$$F_{\rm reg} = \frac{1}{4\pi}\left(\log 4 - \gamma_e - 2\log\eta + \int_0^{\lambda_{0s}/\eta^2} \frac{(e^s-1)}{s}\,ds\right)\,, \tag{3.11b}$$

where γ_e is Euler's constant, while $F_{\rm sing}(r)$ for $r>0$ is given alternatively by

$$F_{\rm sing}(r) = \int_1^\infty e^{-(\xi-1)\kappa} g(\xi)\,d\xi\,, \qquad \textit{where} \quad g(\xi) \equiv \frac{e^{-\kappa+\lambda_{0s}/(\eta^2\xi)}}{4\pi\xi}\,, \quad \textit{with} \quad \kappa \equiv \frac{\eta^2 r^2}{4}\,. \tag{3.11c}$$

To derive (3.11), we must isolate the singularity behavior as $r\to 0$ from $F_{\rm sing}(r)$, as given in (3.8b), by using asymptotics techniques for extracting global contributions from integrals (see chapter 3 of [11]). In (3.8b) we begin by introducing the new variable t by

$$s = -\frac{1}{2}\log r^2 + \frac{1}{2}\log t\,, \tag{3.12}$$

so that $F_{\rm sing}(r)$ in (3.8b) becomes

$$F_{\rm sing}(r) = \frac{1}{4\pi}\int_{\eta^2r^2}^\infty t^{-1}e^{-t/4}e^{\lambda_{0s}r^2/t}\,dt\,. \tag{3.13}$$

Then, by setting $t=\eta^2r^2\xi$ in (3.13) we derive the alternative expression (3.11c) for $F_{\rm sing}(r)$.

The singular behavior in (3.13) as $r\to 0$ occurs from the lower endpoint in (3.13). To isolate this behavior we introduce the intermediate scale δ for which $\eta^2r^2 \ll \delta \ll 1$, so that

$$F_{\rm sing}(r) = \frac{1}{4\pi}\int_{\eta^2r^2}^\delta t^{-1}e^{-t/4}e^{\lambda_{0s}r^2/t}\,dt + \frac{1}{4\pi}\int_\delta^\infty t^{-1}e^{-t/4}e^{\lambda_{0s}r^2/t}\,dt\,. \tag{3.14}$$

In the first integral in (3.14) we can use $e^{-t/4}\sim 1$ since $\eta^2r^2 < t < \delta$ satisfies $t\ll 1$. For the second integral, where $t\geq\delta$, we have $e^{\lambda_{0s}r^2/t}\sim 1$ since $r^2/\delta \ll 1$. In this way, for $r\to 0$ and $\eta^2r^2\ll\delta\ll 1$, we obtain that (3.14) becomes

$$F_{\rm sing}(r) \sim \frac{1}{4\pi}\int_{\eta^2r^2}^\delta t^{-1}e^{\lambda_{0s}r^2/t}\,dt + E_1\left(\delta/4\right)\,, \tag{3.15}$$

where $E_1(w)\equiv\int_w^\infty t^{-1}e^{-t}\,dt$ for $w>0$ is the exponential integral. Upon using the well-known asymptotics $E_1(w)\sim -\log w-\gamma_e$ for $w\to 0^+$, where γ_e is Euler's constant, we obtain that

$$F_{\rm sing}(r) = \frac{1}{4\pi}\int_{\eta^2r^2}^\delta t^{-1}e^{\lambda_{0s}r^2/t}\,dt + \frac{1}{4\pi}\left(\log 4 - \gamma_e - \log\delta\right) + o(1)\,. \tag{3.16}$$

To estimate the integral in (3.16) we introduce a new variable $t=\eta^2r^2\xi$ while adding and subtracting a common term to get

$$F_{\rm sing}(r) = \frac{1}{4\pi}\int_1^{\delta/(\eta^2r^2)} \frac{\left(e^{\lambda_{0s}/(\eta^2\xi)}-1\right)}{\xi}\,d\xi + \frac{1}{4\pi}\int_1^{\delta/(\eta^2r^2)}\frac{1}{\xi}\,d\xi + \frac{1}{4\pi}\left(\log 4-\gamma_e-\log\delta\right)+o(1)\,. \tag{3.17}$$

The first integral on the right hand side of (3.17) is finite as the upper endpoint tends to infinity, i.e. since $\delta \gg \mathcal{O}(r^2)$, while the second integral can be evaluated explicitly. This yields that

$$F_{\text{sing}}(r) = \frac{1}{4\pi}\int_1^\infty \frac{\left(e^{\lambda_{0s}/(\eta^2\xi)}-1\right)}{\xi}\,d\xi + \frac{1}{4\pi}\log\left(\frac{\delta}{\eta^2 r^2}\right) + \frac{1}{4\pi}\left(\log 4 - \gamma_e - \log\delta\right) + o(1)\,. \tag{3.18}$$

In this way, we obtain after cancelling $\log\delta$ terms that

$$F_{\text{sing}}(r) = -\frac{1}{2\pi}\log r + F_{\text{reg}} + o(1)\,, \quad \text{as} \quad r\to 0\,, \tag{3.19a}$$

where F_{reg} is given by

$$F_{\text{reg}} = \frac{1}{4\pi}\left(\log 4 - \gamma_e - 2\log\eta\right) + \frac{1}{4\pi}\int_1^\infty \frac{\left(e^{\lambda_{0s}/(\eta^2\xi)}-1\right)}{\xi}\,d\xi\,. \tag{3.19b}$$

Finally, upon setting $s = \lambda_{0s}/(\eta^2\xi)$ in the integral in (3.19b), we obtain that (3.19b) reduces to the expression for F_{reg} given in (3.11b). Finally, upon using (3.19) in (3.8), we obtain (3.11) from the limiting process in (3.10). This completes the derivation of Principal Result 2.

In Appendix C we provide a different derivation of the limiting behavior (3.19) for $F_{\text{sing}}(r)$ as $r\to 0$. In addition, we provide an alternative integral representation for $F_{\text{sing}}(r)$, valid for $r>0$, than that given in (3.11c)

3.1 Numerical Results

To determine $\lambda_{0s} = \lambda_{0s}(\nu)$ we use Newton's method on (3.7), where the regular part is given in (3.11). The initial guess for the Newton iteration scheme is given by the three-term asymptotic result (2.3) and a numerical Jacobian was used. To approximate the sums over the infinite lattice, we introduce truncations $\bar{\Lambda}$ and $\bar{\Lambda}^\star$ of the direct and reciprocal lattices Λ and $\Lambda^\star$, respectively, which are defined in terms of $M_1>0$ and $M_2>0$ by

$$\bar{\Lambda} \equiv \left\{m\boldsymbol{l}_1 + n\boldsymbol{l}_2 \,\middle|\, -M_1 < m,n < M_1\right\}\,, \quad \bar{\Lambda}^\star \equiv \left\{m\boldsymbol{d}_1 + n\boldsymbol{d}_2 \,\middle|\, -M_2 < m,n < M_2\right\}\,, \quad m,n\in\mathbb{Z}\,. \tag{3.20}$$

The values of M_1 and M_2 were selected so that the absolute value of the increment obtained by increasing M_1 and M_2 by one in the two lattice sums in (3.11a) are each less than 10^{-8}. By choosing the Ewald parameter as $\eta = 2.5$, this truncation criteria yielded (roughly) that $M_1 = 4$ and $M_2 = 3$, which ensures that only a very small number of terms in each of the two infinite sums are required. To numerically evaluate $F_{\text{sing}}(r)$ in (3.11c), we used a Gauss-Laguerre quadrature with $N_q = 200$ nodes. In addition, the integral in (3.11b) that has a removable singularity at $r=0$ was evaluated to high precision using a Gauss-Legendre quadrature.

For a square and hexagonal lattice with a circular trap of radius ε centered at the lattice points, for which $d_c = 1$, in Fig. 3 we compare the numerically-computed result for λ_{0s} with the two-term and three-term asymptotic result, as obtained from (2.3), as ε is varied. Although the three-term result is seen to provide a decent approximation for ε small, the improved result λ_{0s}, which effectively sums all the logarithmic correction terms, provides a significantly better approximation to λ_0 at moderate values of ε.

In Fig. 4 we fix the circular trap radius at $\varepsilon = 0.02$ (left panel) and at $\varepsilon = 0.05$ (right panel) and we compare λ_{0s}, as computed from (3.7), with the two-term and three-term asymptotic results of (2.3) for a one-parameter sweep through the class of Bravais lattices with generators $\boldsymbol{l}_1 = (1/\sqrt{\sin(\theta)}, 0)^T$ and $\boldsymbol{l}_2 = (\cos(\theta)/\sqrt{\sin(\theta)}, \sqrt{\sin(\theta)})^T$ on the

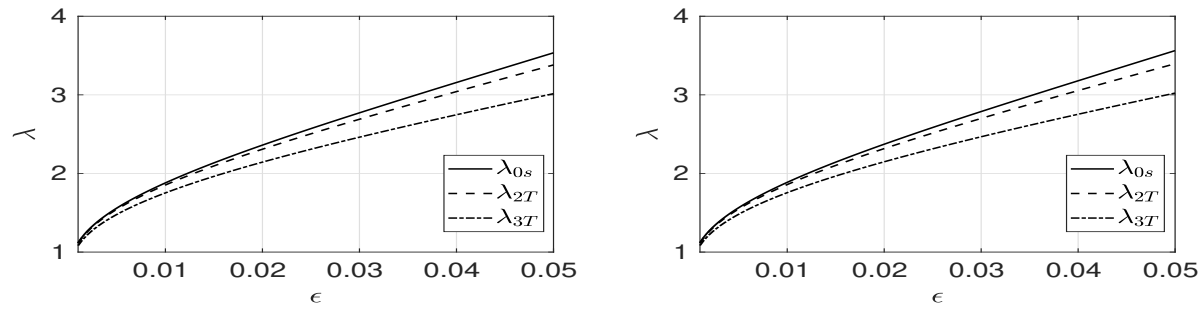

Figure 3: The asymptotic result λ_{0s} computed from (3.7), which is accurate to all orders in ν, is compared with the two-term λ_{2T} and three-term λ_{3T} result, as obtained from (2.3), for a circular trap of radius ε. As the trap radius increases, the three-term result deviates from λ_{0s}. Left panel: square lattice. Right panel: hexagonal lattice. The results are very similar for both lattices.

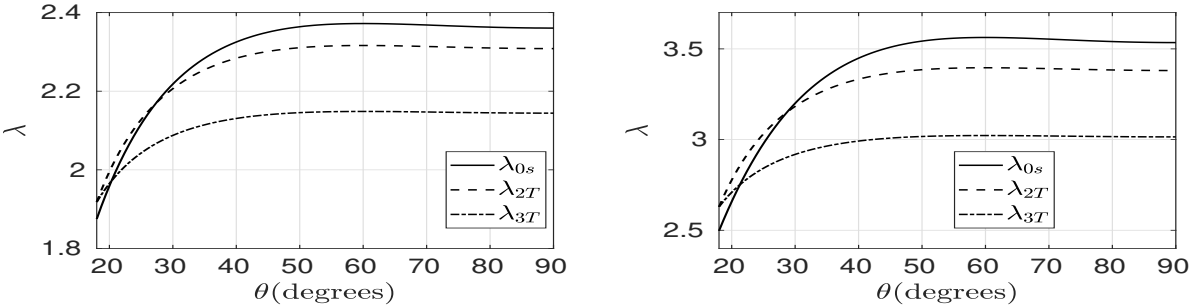

Figure 4: For a circular trap of radii $\varepsilon = 0.02$ (left panel) and $\varepsilon = 0.05$ (right panel), the asymptotic result λ_{0s}, computed from (3.7), is compared with the two and three-term asymptotic results, as obtained from (2.3) for a one-parameter sweep through the class of Bravais lattices with generators $\boldsymbol{l}_1 = (1/\sqrt{\sin(\theta)}, 0)^T$ and $\boldsymbol{l}_2 = (\cos(\theta)/\sqrt{\sin(\theta)}, \sqrt{\sin(\theta)})^T$ on the range $\pi/10 \leq \theta \leq \pi/2$. We observe that λ_{0s} is maximized for the hexagonal lattice with $\pi/3$.

range $\pi/10 \leq \theta \leq \pi/2$. From this figure, we observe that λ_{0s}, and not just the two-term expansion, is maximized for a hexagonal lattice.

The results shown in Fig. 3 and Fig. 4 for a circular trap of radius ε also apply to a trap of arbitrary shape by simply relabeling the horizontal axes in these figures by εd_c. The logarithmic capacitance d_c for Ω_0, as defined by the canonical problem (2.4), depends on the shape of Ω_0 but is invariant under rotations of Ω_0. In Table 1, numerical values for d_c are given for various specific trap shapes Ω_1 (cf. [27]). For a general trap shape, a boundary integral numerical method, such as described in [8], can be used to numerically compute d_c.

4 Transcendentally small effects

In this section, we determine transcendentally small corrections in the asymptotic approximation of the principal eigenvalue λ_0 for (1.2). For a general trap shape Ω_0, the dipole term in the canonical inner problem (2.4) determines that the correction term for the eigenfunction in the outer region is $\mathcal{O}(\epsilon)$. As such, we expand the principal eigenvalue and its corresponding eigenfunction in the outer region as

$$\lambda_0 \sim \lambda_{0s}(\nu) + \varepsilon\lambda_{1s}(\nu) + \cdots ; \qquad \Phi = \Phi_{0s}(\boldsymbol{x};\nu) + \varepsilon\Phi_{1s}(\boldsymbol{x};\nu) + \cdots . \tag{4.1}$$

Shape of $\Omega_0 \equiv \varepsilon^{-1}\Omega_\varepsilon$	Logarithmic capacitance d_c
circle, radius a	$d_c = a$
ellipse, semi-axes a, b	$d_c = \frac{a+b}{2}$
equilateral triangle, sidelength h	$d_c = \frac{\sqrt{3}\,\Gamma\left(\frac{1}{3}\right)^3 h}{8\pi^2} \approx 0.422h$
isosceles right triangle, short side h	$d_c = \frac{3^{3/4}\Gamma\left(\frac{1}{4}\right)^2 h}{2^{7/2}\pi^{3/2}} \approx 0.476h$
square, sidelength h	$d_c = \frac{\Gamma\left(\frac{1}{4}\right)^2 h}{4\pi^{3/2}} \approx 0.5902h$

Table 1: The logarithmic capacitance d_c for some cross-sectional shapes of $\Omega_0 \equiv \varepsilon^{-1}\Omega_\varepsilon$.

The inner solution $v = \Phi(\varepsilon y) \sim A v_c(\boldsymbol{y})$, where v_c satisfies (2.4) with far-field behavior (2.8), yields the following matching condition for the outer solution Φ as $\boldsymbol{x} \to \mathbf{0}$:

$$\Phi = A\log|\boldsymbol{x}| + \frac{A}{\nu} + \varepsilon A\frac{\boldsymbol{p}_c\cdot\boldsymbol{x}}{|\boldsymbol{x}|^2} + \mathcal{O}(\varepsilon^2)\,. \tag{4.2}$$

Upon substituting (4.1) into (1.2), and collecting $\mathcal{O}(\varepsilon)$ terms in (1.2) and (4.2), we obtain that Φ_{1s} satisfies

$$\Delta\Phi_{1s} + \lambda_{0s}\Phi_{1s} = -\lambda_{1s}\Phi_{0s}\,, \quad \boldsymbol{x}\in\Omega\backslash\{\mathbf{0}\}\,; \qquad \Phi_{1s}\in\mathcal{P}\,, \quad \boldsymbol{x}\in\partial\Omega\,, \tag{4.3a}$$

$$\Phi_{1s} \sim A\frac{\boldsymbol{p}_c\cdot\boldsymbol{x}}{|\boldsymbol{x}|^2} \quad \text{as} \quad \boldsymbol{x}\to\mathbf{0}\,; \qquad \int_\Omega \Phi_{1s}\Phi_{0s}\,d\boldsymbol{x} = 0\,. \tag{4.3b}$$

To determine λ_{1s} we apply Green's second identity to the PDE's (3.4) and (4.3) for Φ_{0s} and Φ_{1s} over the region $\Omega\backslash\mathcal{B}_\mu$, where $\mathcal{B}_\mu$ is a disk of radius $\mu > 0$ centered at $\boldsymbol{x} = \mathbf{0}$. By using the periodicity condition on $\partial\Omega$, we derive

$$\lambda_{1s}\int_{\Omega\backslash\mathcal{B}_\mu}\Phi_{0s}^2\,d\boldsymbol{x} = \int_{\partial\mathcal{B}_\mu}\left(\Phi_{1s}\partial_n\Phi_{0s} - \Phi_{0s}\partial_n\Phi_{1s}\right)ds\,, \tag{4.4}$$

where the outward normal derivative ∂_n points into the disk $\mathcal{B}_\mu$. Taking the limit $\mu\to 0^+$ in (4.4), while using $\int_\Omega \Phi_{0s}^2\,d\boldsymbol{x} = 1$ and $\partial_n = -\partial_r$ with $r \equiv |\boldsymbol{x}| = \mu$ on $\partial\mathcal{B}_\mu$, we obtain that

$$\lambda_{1s} = \lim_{\mu\to 0}\int_0^{2\pi}\left(\Phi_{0s}\partial_r\Phi_{1s} - \Phi_{1s}\partial_r\Phi_{0s}\right)\Big|_{r=\mu}\mu\,ds\,. \tag{4.5}$$

Since $\Phi_{0s} = -2\pi A G_\lambda(\boldsymbol{x})$, we use the local behavior as $\boldsymbol{x}\to\mathbf{0}$ for G_λ in (3.6b), together with (4.3b) for Φ_{1s}, to calculate on $r = \mu$ with $\mu \ll 1$ that

$$\Phi_{0s} = A\log\mu - 2\pi A R_\lambda + \mathcal{O}(\mu^2\log\mu)\,, \quad \partial_r\Phi_{0s} = \frac{A}{\mu} + \mathcal{O}(\mu\log\mu)\,, \quad \Phi_{1s}\sim A\frac{\boldsymbol{p}_c\cdot\boldsymbol{e}}{\mu}\,, \quad \partial_r\Phi_{1s}\sim -A\frac{\boldsymbol{p}_c\cdot\boldsymbol{e}}{\mu^2}\,, \tag{4.6}$$

where $\boldsymbol{e} \equiv (\cos\theta, \sin\theta)^T$. Upon substituting (4.6) into (4.5), we use $\int_0^{2\pi}\boldsymbol{p}_c\cdot\boldsymbol{e}\,d\theta = 0$ to conclude that $\lambda_{1s} = 0$. With $\lambda_{1s} = 0$, we can write the problem (4.3) for Φ_{1s} as

$$\Delta\Phi_{1s} + \lambda_{0s}\Phi_{1s} = 2\pi A\boldsymbol{p}_c\cdot\nabla_{\boldsymbol{x}}\delta(\boldsymbol{x})\,, \quad \boldsymbol{x}\in\Omega\,; \qquad \Phi_{1s}\in\mathcal{P}\,, \quad \boldsymbol{x}\in\partial\Omega\,; \qquad \int_\Omega\Phi_{1s}\Phi_{0s}\,d\boldsymbol{x} = 0\,. \tag{4.7}$$

As such, for a general trap shape, we conclude that $\lambda_0 \sim \lambda_{0s} + o(\varepsilon)$.

Although it is challenging to explicitly determine the first non-vanishing correction to λ_{0s} for an arbitrary trap shape, we now show how to determine this eigenvalue correction for the special case where the trap Ω_ε is a disk of radius ε. For this trap shape, we have $d_c = 1$, $\boldsymbol{p}_c = \mathbf{0}$, $\Phi_{1s}\equiv 0$ from (4.7), and $v_c = \log|\boldsymbol{y}|$ for $|\boldsymbol{y}| \geq 1$. The following more refined result for the local behavior of $G_\lambda(\boldsymbol{x})$ as $\boldsymbol{x}\to\mathbf{0}$ is essential for the higher-order analysis below:

Lemma 1 *In the limit $\boldsymbol{x} \to 0$, the Helmholtz Green's function $G_\lambda(\boldsymbol{x})$, which satisfies (3.6), has the local behavior*

$$G_\lambda = -\frac{1}{2\pi}\log|\boldsymbol{x}| + R_\lambda + \frac{\lambda_{0s}}{8\pi}|\boldsymbol{x}|^2\log|\boldsymbol{x}| - \left(\frac{\lambda_{0s}}{8\pi} + \frac{\lambda_{0s}R_\lambda}{4}\right)|\boldsymbol{x}|^2 + \mathcal{H}_{11}x_1^2 + 2\mathcal{H}_{12}x_1x_2 + \mathcal{H}_{22}x_2^2 + o(|\boldsymbol{x}|^2)\,, \tag{4.8}$$

where $\boldsymbol{x} = (x_1, x_2)^T$. Here, $\mathcal{H}_{11}$, $\mathcal{H}_{12}$, and $\mathcal{H}_{12}$ are constants with $\mathcal{H}_{11} + \mathcal{H}_{22} = 0$.

To derive (4.8) we use a dominant balance argument. For $r = |\boldsymbol{x}| \ll 1$, we set

$$G_\lambda = -\frac{1}{2\pi}\log r + R_\lambda + c_0 r^2\log r + c_1 r^2 + \mathcal{H}(\boldsymbol{x})\,, \tag{4.9}$$

in (3.6) to obtain after a short calculation that

$$\Delta\mathcal{H} + \lambda_{0s}\mathcal{H} = \left(\frac{\lambda_{0s}}{2\pi} - 4c_0\right)\log r - (4c_1 + 4c_0 + \lambda_{0s}R_\lambda) - c_0\lambda_{0s}r^2\log r - \lambda_{0s}c_1 r^2\,. \tag{4.10}$$

By eliminating the coefficients of the logarithmic and the constant term on the right-hand side of (4.10) we conclude that $c_0 = \lambda_{0s}/(8\pi)$ and $c_1 = -c_0 - \lambda_{0s}R_\lambda/4$. With these choices, we obtain that $\Delta\mathcal{H} + \lambda_{0s}\mathcal{H} = \mathcal{O}(r^2\log r)$ as $r \to 0$. The most general solution for $\mathcal{H}$ with $\mathcal{H} = \mathcal{O}(|\boldsymbol{x}|^2)$ as $\boldsymbol{x} \to \boldsymbol{0}$ has the form $\mathcal{H} = \mathcal{H}_{11}x_1^2 + 2\mathcal{H}_{12}x_1x_2 + \mathcal{H}_{22}x_2^2 + o(|\boldsymbol{x}|^2)$, where $\mathcal{H}_{11} + \mathcal{H}_{22} = 0$. With c_0, c_1, and $\mathcal{H}$ determined in this way, we obtain the local expansion (4.8) from (4.9). We remark that the coefficients $\mathcal{H}_{11}$, $\mathcal{H}_{22}$, and $\mathcal{H}_{12}$ are global quantities that depend on the particular lattice and their values can not be determined from a local analysis.

For a circular trap of radius ε, for which $d_c = 1$, we recall from (3.7) that λ_{0s} is the smallest positive root of $R_\lambda = (2\pi)^{-1}\log\varepsilon$ (see (3.7)). By setting $\boldsymbol{x} = \varepsilon\boldsymbol{y}$ and $R_\lambda = (2\pi)^{-1}\log\varepsilon$ in (4.8), we readily derive in terms of the inner variable $|\boldsymbol{y}|$ that

$$G_\lambda \sim -\frac{1}{2\pi}\log|\boldsymbol{y}| + \frac{\varepsilon^2\lambda_{0s}}{8\pi}\left(|\boldsymbol{y}|^2\log|\boldsymbol{y}| - |\boldsymbol{y}|^2\right) + \frac{\varepsilon^2|\boldsymbol{y}|^2}{2}\left(\mathcal{H}_{11} - \mathcal{H}_{22}\right)\cos(2\theta) + \varepsilon^2\mathcal{H}_{12}|\boldsymbol{y}|^2\sin(2\theta)\,, \tag{4.11}$$

where $\boldsymbol{y} = |\boldsymbol{y}|(\cos\theta, \sin\theta)^T$.

Next, we use (4.11) to perform a higher-order matching between the inner and outer expansions for the eigenfunction for the case of a circular trap. We expand the eigenvalue and the eigenfunction in the outer region as

$$\lambda_0 \sim \lambda_{0s}(\nu) + \varepsilon^2\lambda_{2s}(\nu) + \cdots\,; \qquad \Phi = \Phi_{0s}(\boldsymbol{x};\nu) + \varepsilon^2\Phi_{2s}(\boldsymbol{x};\nu) + \cdots\,, \tag{4.12}$$

where $\Phi_{0s} = -2\pi A G_\lambda(\boldsymbol{x})$. In the inner region, we expand $v(\boldsymbol{y}) = \Phi(\varepsilon\boldsymbol{y})$ as

$$v(\boldsymbol{y}) = A v_c(\boldsymbol{y}) + \varepsilon^2 v_1(\boldsymbol{y}) + \cdots\,, \tag{4.13}$$

where $v_c(\boldsymbol{y}) = \log|\boldsymbol{y}|$. We substitute (4.13) into (1.2), while using the coefficient of the $\mathcal{O}(\varepsilon^2)$ term in (4.11) to determine the far-field behavior of $v_1(\boldsymbol{y})$. In this way, we obtain that v_1 satisfies

$$\begin{aligned} &\Delta_{\boldsymbol{y}} v_1 = -\lambda_{0s}A v_c(\boldsymbol{y})\,, \quad \text{in} \quad |\boldsymbol{y}| \ge 1\,; \qquad v_1 = 0\,, \quad \text{on} \quad |\boldsymbol{y}| = 1\,, \\ &v_1 \sim -\frac{A\lambda_{0s}}{4}\left(|\boldsymbol{y}|^2\log|\boldsymbol{y}| - |\boldsymbol{y}|^2\right) - \pi A|\boldsymbol{y}|^2\left[\left(\mathcal{H}_{11} - \mathcal{H}_{22}\right)\cos(2\theta) + \mathcal{H}_{12}\sin(2\theta)\right]\,, \quad \text{as} \quad |\boldsymbol{y}| \to \infty\,. \end{aligned} \tag{4.14}$$

The exact solution to this problem is

$$v_1 = -\frac{A\lambda_{0s}}{4}\left(|\boldsymbol{y}|^2\log|\boldsymbol{y}| + 1 - |\boldsymbol{y}|^2\right) - \pi A\left(|\boldsymbol{y}|^2 - \frac{1}{|\boldsymbol{y}|^2}\right)\left[\left(\mathcal{H}_{11} - \mathcal{H}_{22}\right)\cos(2\theta) + \mathcal{H}_{12}\sin(2\theta)\right]\,. \tag{4.15}$$

Letting $|\boldsymbol{y}| \to \infty$ in (4.15), and recalling the inner expansion (4.13), we obtain that there is an unmatched term $-\varepsilon^2 A\lambda_{0s}/4$, which must be accounted for by the outer expansion (4.12). In this way, by substituting (4.12) into (1.2) we conclude that Φ_{2s} satisfies

$$\Delta\Phi_{2s} + \lambda_{0s}\Phi_{2s} = -\lambda_{2s}\Phi_{0s}\,, \quad \boldsymbol{x} \in \Omega\backslash\{\mathbf{0}\}\,; \qquad \Phi_{2s} \in \mathcal{P}\,, \quad \boldsymbol{x} \in \partial\Omega\,, \tag{4.16a}$$

$$\Phi_{2s} \sim -\frac{A\lambda_{0s}}{4} \quad \text{as} \quad \boldsymbol{x} \to \mathbf{0}\,; \qquad \int_\Omega \Phi_{2s}\Phi_{0s}\,d\boldsymbol{x} = 0\,. \tag{4.16b}$$

Next, as similar to the derivation of (4.5), we obtain from Green's identity applied to Φ_{0s} and Φ_{2s} that

$$\lambda_{2s} = \lim_{\mu\to 0}\int_0^{2\pi} (\Phi_{0s}\partial_r\Phi_{2s} - \Phi_{2s}\partial_r\Phi_{0s})\Big|_{r=\mu}\mu\,ds\,. \tag{4.17}$$

By using (4.6) for Φ_{0s} on $r = \mu \ll 1$, together with the local behavior (4.16b) for Φ_{2s}, we readily calculate from (4.17) that

$$\lambda_{2s} = \frac{\pi A^2\lambda_{0s}}{2}\,, \tag{4.18}$$

where A is given in (3.5). We summarize our result as follows:

Principal Result 3 *For $\varepsilon \to 0$, the asymptotic expansion for the principal eigenvalue λ_0 for (1.2) for an arbitrary oblique Bravais lattice, and with a circular trap of radius ε centered at each of the lattice points, is*

$$\lambda_0 \sim \lambda_{0s} + \frac{\varepsilon^2\lambda_{0s}}{8\pi}\left[\int_\Omega G_\lambda^2\,d\boldsymbol{x}\right]^{-1} + \cdots\,. \tag{4.19a}$$

Here λ_{0s} is the smallest positive root of $R_\lambda = (2\pi)^{-1}\log\varepsilon$. By estimating the integral in (4.19a), we obtain the explicit approximation

$$\lambda_0 = \lambda_{0s} + \varepsilon^2\pi^2\nu^3\left[1 - 6\pi\nu R_p + \mathcal{O}(\nu^2)\right]\,, \qquad \textit{with} \quad \nu = -1/\log\varepsilon\,, \tag{4.19b}$$

where R_p is the regular part of the periodic source-neutral Green's function, as given in (2.2b) for an arbitrary Bravais lattice.

To derive (4.19b) from (4.19a), we use the $\lambda_{0s} \ll 1$ approximation in the PDE (3.6) to readily calculate that

$$G_\lambda = -\frac{1}{\lambda_{0s}} + G_p + \mathcal{O}(\lambda_{0s})\,, \tag{4.20}$$

where G_p is the periodic source-neutral Green's function satisfying (2.1), and given explicitly by (2.2). Since $\int_\Omega G_p\,d\boldsymbol{x} = 0$, we obtain for $\lambda_{0s} \ll 1$ that

$$\int_\Omega G_\lambda^2\,d\boldsymbol{x} = \frac{1}{\lambda_{0s}^2} + \mathcal{O}(1)\,, \qquad \text{so that} \qquad \frac{\lambda_{0s}}{8\pi}\left[\int_\Omega G_\lambda^2\,d\boldsymbol{x}\right]^{-1} = \frac{\lambda_{0s}^3}{8\pi}\left(1 - \mathcal{O}(\lambda_{0s}^2)\right)\,. \tag{4.21}$$

Finally, the explicit result (4.19b) is obtained by substituting $\lambda_{0s} \sim 2\pi\nu - 4\pi^2 R_p\nu^2$, as given in (2.3), into the last relation in (4.21) where $\nu \equiv -1/\log\varepsilon$.

4.1 Numerical Validation of Asymptotic Theory

In this sub-section we compare our asymptotic approximations for the fundamental eigenvalue of (1.2) for a circular trap of radius ε centered at the lattice points with corresponding numerical results computed from FlexPDE [9]. The FlexPDE computations are done in both a square and a regular hexagonal FWS cell with periodic boundary conditions. Although it is straightforward to solve eigenvalue problems with FlexPDE [9], here we have the additional challenge that version 6.50 of FlexPDE, which we are using, does not fully support multiple periodic boundary conditions. Hence, care must be taken in imposing boundary conditions at the domain vertices to avoid mapping them to two different points. To circumvent this difficulty, very small segments with homogeneous Neumann boundary conditions must be added before and after each vertex. We chose the length of such segment to be $\rho \approx 0.001$, which results in a very fine mesh at the corners (in addition to the region near the trap). For both the square and hexagonal lattices, and for a few different radii of the circular traps, in Table 2 we give the asymptotic predictions based on the three-term approximation from (2.3), the log-summed approximation from (3.7) and (3.11), and the improved approximation in (4.19b) as obtained by including the first transcendentally small terms. The corresponding FlexPDE results are given in the last column of Table 2. From this table, we observe a very close agreement between the FlexPDE results and both the log-summed and improved approximation when ε is small. Even at the moderately large value $\varepsilon = 0.1$, the error in using the improved approximation (4.19b) is only roughly 4.5%. In contrast, while the three-term result (2.3) provides only a decent approximation when ε is very small, the agreement with the FlexPDE result is rather poor when $\varepsilon = 0.1$. These results show that from a simple Newton iteration based on (3.7) and (3.11) a rather accurate approximation for the principal eigenvalue can be achieved even for only moderately small ε. We emphasize that such approximation can be done for an arbitrary Bravais lattice. For $\varepsilon = 0.05$, in Fig. 5 we give contour plots of the eigenfunction associated with the first eigenvalue in both the square (left panel) and the hexagonal (right panel) FWS cells.

ε	Lattice	λ_{3T}	λ_{0s}	(4.19b)	λ_{0N} (FlexPDE)
0.01	square	1.8533	1.880026	1.880044	1.880017
0.02	square	2.3084	2.360634	2.360766	2.360766
0.03	square	2.6896	2.771263	2.771799	2.771913
0.05	square	3.3806	3.534722	3.536845	3.538754
0.10	square	5.0872	5.500804	5.522693	5.559822
0.01	hexagon	1.8586	1.887048	1.887078	1.887050
0.02	hexagon	2.3163	2.372161	2.372294	2.372306
0.03	hexagon	2.6999	2.787662	2.788101	2.788325
0.05	hexagon	3.3960	3.562928	3.565060	3.567066
0.10	hexagon	5.1173	5.577959	5.599959	5.639788

Table 2: Comparison of the three-term λ_{3T} result (see (2.3)), the log-summed approximation λ_{0s}, the improved approximation (4.19b) with a few transcendentally small terms, and the full numerical FlexPDE [9] result λ_{0N} for the principal eigenvalue of (1.2). For the FlexPDE numerical computation we set the error tolerance to be 1×10^{-5}, which controls the number of successive mesh refinement before providing the solution. The trap is circular with radius ε and is centered at the origin of the FWS cell for the lattice.

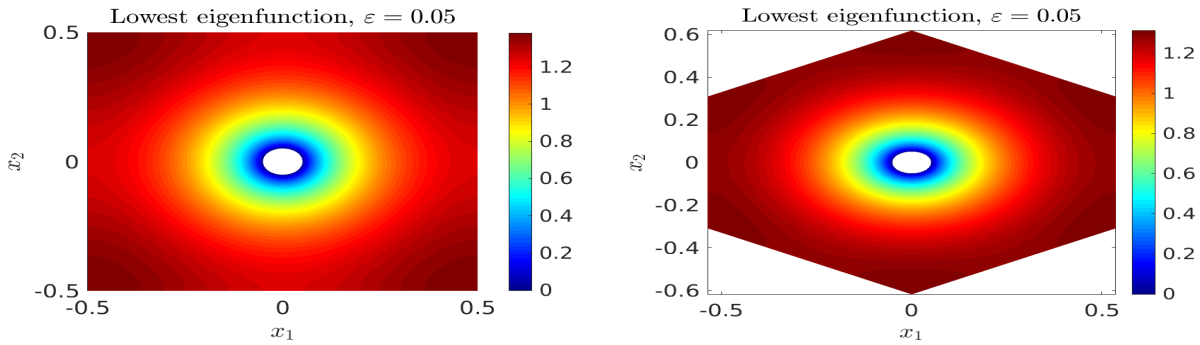

Figure 5: Contour plot of the FlexPDE [9] numerically-computed eigenfunction corresponding to the principal eigenvalue of (1.2) in the FWS cell given by the unit square (left panel) and the regular hexagon (right panel), each of unit area, for a square and hexagonal lattice of traps, respectively. A circular trap of radius $\varepsilon = 0.05$ is centered at the origin.

4.2 Numerical calculation of the logarithmic capacitance and dipole of a trap cluster

When the trap set Ω_0 consists of a collection of $m > 1$ non-overlapping disks, the simple numerical approach of [14], as inspired by the methodology introduced in [31], can be used to numerically estimate the logarithmic capacitance d_c and dipole vector $\boldsymbol{p}_c$ from (2.4).

The approach of [31] is based on using a series solution to Laplace's equation with unknown coefficients. By using a least-squares fit to the homogeneous Dirichlet condition on the boundary of each circular trap, the coefficients in the series are then estimated numerically. In [14], v_c was taken to have the form (see also equations (3.1) and (3.2) of [31])

$$v_c(z) = -\log d_c + \sum_{j=1}^{m} e_j \log|z - c_j| + \sum_{j=1}^{m}\sum_{k=1}^{n} \left(a_{jk}\,\mathrm{Re}(z-c_j)^{-k} + b_{jk}\,\mathrm{Im}(z-c_j)^{-k} \right), \tag{4.22}$$

where we impose the additional condition that $\sum_{j=1}^{m} e_j = 1$. In (4.22), $z \in \mathbb{C}$ corresponds to the point $\boldsymbol{y}$ in complex coordinates, $c_j \in \mathbb{C}$ is the center of the j^{th} trap in the cluster, and m is the number of traps in the cluster. The real-valued constants $\log d_{1c}$, e_j, a_{jk}, and b_{jk} for $j = 1, \ldots, m$ and $k = 1, \ldots, n$ are determined so that the boundary condition $v_c = 0$ on each trap is satisfied in the sense of least-squares. By imposing $v_c(z) = 0$ at $3n$ uniformly spaced points on the boundary of each trap, a $3nm + 1$ linear algebraic system of equations is obtained with $(2nm + m + 1)$ unknowns. The backslash command in MATLAB [22] is then used to numerically perform the least-squares fit. In our computations below we show that $n = 10$ yields highly accurate results when compared with exact solutions that are available for a two-trap cluster.

Next, we show how to identify an approximation to the dipole term in (2.4). For $|z| \gg 1$, we use the estimates

$$\log|z - c_j| = \log|z| - \frac{\mathrm{Re}(z\bar{c}_j)}{|z|^2} + \mathcal{O}(|z|^{-2}), \qquad \mathrm{Re}(z-c_j)^{-1} \sim \frac{\mathrm{Re}(z)}{|z|^2}, \qquad \mathrm{Im}(z-c_j)^{-1} \sim \frac{\mathrm{Im}(\bar{z})}{|z|^2}, \tag{4.23}$$

in (4.22) to obtain for $|z| \gg 1$, with $z = y_1 + iy_2$, that

$$v_c \sim \log|\boldsymbol{y}| - \log d_c + \frac{\hat{\boldsymbol{p}}_c \cdot \boldsymbol{y}}{|\boldsymbol{y}|^2} + \cdots, \qquad \hat{\boldsymbol{p}}_c \equiv \left(\sum_{j=1}^{m} (a_{j1} - e_j \mathrm{Re}(\bar{c}_j)), -\sum_{j=1}^{m} (b_{j1} - e_j \mathrm{Im}(\bar{c}_j)) \right). \tag{4.24}$$

In this way, $\hat{\boldsymbol{p}}_c$ is the numerical approximation to the dipole vector $\boldsymbol{p}_c$ in (2.4).

Figure 6: Left panel: two circular traps each of unit radius in the inner region with center-to-center separation l_c. Right panel: a three-trap cluster with traps each of unit radius centered at $(l_c, 0)$ and $\left(-\sqrt{3}l_c/2, \pm l_c/2\right)$.

We now use this simple numerical approach to approximate d_c and $\boldsymbol{p}_c$ for the two- and three-trap clusters of circular traps of a common radius as shown in Fig. 6. For the two-trap case, where there are two lines of symmetry through the origin, we conclude that $\boldsymbol{p}_c \equiv \boldsymbol{0}$. By solving (2.4) using bipolar coordinates as in Appendix A of [19], the logarithmic capacitance of a two-trap cluster having a center-to-center separation $l_c > 2$ is

$$\log d_c = \frac{1}{2}\log\left(l_c^2 - 4\right) - \frac{\beta}{2} + \sum_{k=1}^{\infty} \frac{e^{-k\beta}}{k\cosh(k\beta)}\,, \qquad \beta \equiv \cosh^{-1}\left(l_c/2\right)\,. \tag{4.25}$$

In Fig. 7 we compare the analytical result for d_c for a two-trap cluster with the corresponding numerical result computed from (4.22) on the range $l_c > 2$ with $n = 10$. From the right panel of Fig. 7 we observe that the numerical result predicts the analytical result for d_c in (4.25) with high precision on the entire range $l_c > 2$. For the two-trap cluster, our numerical approximation in (4.24) for the dipole vector yields that $|\hat{\boldsymbol{p}}_c| \approx 10^{-15}$.

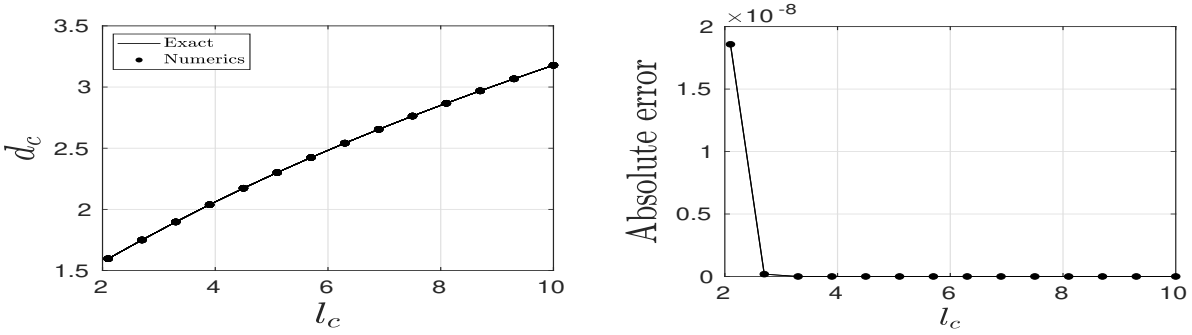

Figure 7: Comparison of analytical and numerical result for d_c versus l_c for a two-trap cluster with disks of a common unit radius in the inner coordinate. The right panel, showing the error in the approximation, indicates that the numerical result based on (4.22) with $n = 10$ provides a highly accurate determination of d_c.

In Fig. 8 we plot the numerical approximation for d_c and the x-component of the dipole vector $\boldsymbol{p}_c$ for the three-trap cluster shown in the right panel of Fig. 6 as $l_c > 1$ is varied. Theoretically, since the three-trap cluster is symmetric about the line $y_2 = 0$, it follows that the y-component p_{cy} of the dipole vector must vanish. Our numerical results yield that $\hat{p}_{cy} \approx 10^{-15}$ on the range $l_c > 1$.

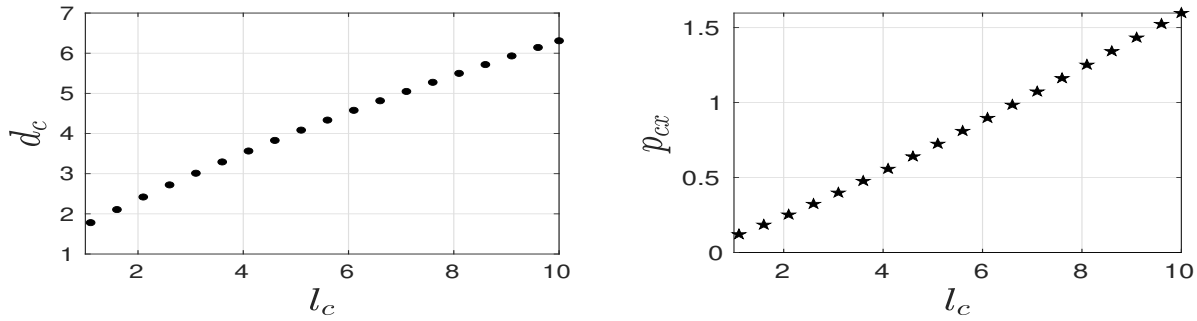

Figure 8: The numerical approximation, obtained from (4.22) and (4.24), for the logarithmic capacitance d_c (left panel) and for the x-component p_{cx} (right panel) of the dipole vector $\boldsymbol{p}_c = (p_{cx}, 0)^T$ as $l_c > 1$ is varied for the three-trap cluster shown in the right panel of Fig. 6.

5 Discussion

The goal of this paper was to derive and numerically evaluate asymptotic approximations, of various accuracy, for the principal eigenvalue of the Laplacian with a periodic arrangement of localized traps of spatial extent $\mathcal{O}(\varepsilon)$ centered at the lattice points of an arbitrary Bravais lattice in $\mathbb{R}^2$. In our analysis, the traps can either be isolated or within a trap cluster, and they are characterized by the logarithmic capacitance d_c associated with the far-field behavior of the canonical problem (2.4) defined near the trap set. We showed how to obtain accurate numerical solutions for d_c when the trap set consists of a collection of non-overlapping disks.

For $\varepsilon \to 0$, in Principal Result 1 we derived a three-term approximation in powers of $\nu = -1/\log(\varepsilon d_c)$ for this principal eigenvalue. The lattice-dependent coefficients in this series were readily evaluated numerically using an explicit formula in [6] for the source-neutral periodic Green's function and its regular part. Next, we obtained a much improved approximation for the principal eigenvalue, which captures all of the logarithmic terms in powers of ν, from applying a simple Newton iteration scheme to a transcendental equation involving the regular part of the periodic Helmholtz Green's function. For the viability of this approach, it was critical to extend the methodology of [2] to provide a rapidly converging infinite series representation for the regular part of this Green's function for an arbitrary Bravais lattice. Based on comparisons of our approximations for the principal eigenvalue with corresponding full numerical results from the PDE eigenvalue problem, we showed that while the three-term asymptotic approximation agrees well with the numerical result only for a rather small trap radius, the asymptotic result based on the transcendental equation provides a highly accurate prediction of the principal eigenvalue even for only a moderately small trap radius. Although we have focused only on the lowest eigenvalue, we remark that the approach used in § 3 can also be used to calculate the perturbation for the higher eigenvalues.

As an extension to this study, it would be worthwhile to derive an analogous expression to that in (3.11) of Principal Result 2 for the regular part of the quasi-periodic Helmholtz Green's function for an arbitrary Bravais lattice. In this way, one could calculate accurate approximations for the effect of the trap on various Bloch modes as the Bloch wavenumber is varied. We remark that an expression similar to (3.11) was derived recently in [13] for the the regular past of the reduced-wave Bloch Green's function.

Finally, we remark that the transcendental equation (3.7) for the log-summed approximation to the principal

eigenvalue of the Laplacian still applies for other types of defects, but with a different expression for d_c. As an illustration of this, suppose that the hole in (1.2) is replaced by a localized compactly-supported piecewise-constant potential centered at the lattice points, so that in the FWS cell we have the following eigenvalue problem with $\varepsilon \ll 1$:

$$\triangle\Phi + \left(\lambda + \varepsilon^{-2} W\left[\varepsilon^{-1}|\boldsymbol{x}|\right]\right)\Phi = 0\,, \quad \boldsymbol{x}\in\Omega\,; \qquad \Phi\in\mathcal{P}\,, \quad \boldsymbol{x}\in\partial\Omega\,; \qquad W(\rho)\equiv\begin{cases} 0\,, & \rho>1\,,\\ W_0\,, & 0\le\rho<1\,,\end{cases} \tag{5.1}$$

where W_0 is a constant. The corresponding radially symmetric inner problem, which replaces (2.4), is now

$$v_c'' + \rho^{-1}v_c' + W(\rho)v_c = 0\,, \quad \rho\ge 0\,; \qquad v_c = \log\rho - \log d_c + o(1)\,, \quad \text{as} \quad \rho\to\infty\,. \tag{5.2}$$

The constant d_c in (5.2) is readily calculated from the explicit solution to (5.2) by imposing C^1 continuity of v_c across $\rho=1$. In this way, we obtain that the transcendental equation (3.7) still holds, but where d_c is now given by

$$\log d_c = -\frac{J_0(\sqrt{V_0})}{\sqrt{V_0}J_0'(\sqrt{V_0})}\,, \quad \text{for} \quad 0<V_0<z_0^2\,; \qquad \log d_c = -\frac{I_0(\sqrt{|V_0|})}{\sqrt{|V_0|}I_0'(\sqrt{|V_0|})}\,, \quad \text{for} \quad V_0<0\,. \tag{5.3}$$

Here $J_0(z)$ and $I_0(z)$ are the Bessel and modified Bessel functions of the first kind of order zero, respectively, and z_0 is the first positive root of $J_0'(z)=0$. Vibration problems with strongly concentrated masses or electromagnetic resonance problems with a localized, but high contrast, dielectric imperfection, can be treated in a similar way (cf. [28]).

Acknowledgements

Michael Ward gratefully acknowledges the financial support from the NSERC Discovery Grant Program.

Appendices

A Formulation on the fundamental Wigner Seitz cell

In this appendix, we provide a more refined description of the FWS cell, as was discussed in §2.2 of [12]. For a general Bravais lattice, there are eight nearest neighbor lattice points to $\boldsymbol{x}=\mathbf{0}$ given by the set

$$P\equiv\{\, m\boldsymbol{l}_1 + n\boldsymbol{l}_2 \,|\, m\in\{0,1,-1\}\,,\ n\in\{0,1,-1\}\,,\ (m,n)\neq 0\}\,. \tag{A.4}$$

For each (vector) point $\boldsymbol{P}_i\in P$, for $i=1,\dots,8$, the Bragg line L_i is defined as the line that crosses the point $\boldsymbol{P}_i/2$ orthogonally to $\boldsymbol{P}_i$. The unit outer normal to L_i is labeled by $\boldsymbol{\eta}_i\equiv\boldsymbol{P}_i/|\boldsymbol{P}_i|$. The convex hull generated by these Bragg lines is the FWS cell Ω. Specifically, for the hexagonal lattice (1.1) its boundary $\partial\Omega$ is the union of exactly six Bragg lines, while for a square lattice the boundary of $\partial\Omega$ consists of four Bragg lines. Generically, for an oblique Bravais lattice, $\partial\Omega$ is the union of six Bragg lines. The centers of the Bragg lines generating $\partial\Omega$ are re-indexed as $\boldsymbol{P}_i/2$ for $i=1,\dots,L$, where $L\in\{4,6\}$. The boundary $\partial\Omega$ of Ω is the union of the re-indexed Bragg lines L_i for $i=1,\dots,L$. The boundary $\partial\Omega$ is then parameterized segment-wise as

$$\partial\Omega = \left\{\boldsymbol{x}\in\bigcup_i\{\frac{\boldsymbol{P}_i}{2}+t\boldsymbol{\eta}_i^{\perp}\}\ \Big|\ -t_i\le t\le t_i\,,\ \ i=1,\dots,L\,,\ \ L\in\{4,6\}\right\}. \tag{A.5}$$

Here $2t_i$ is the length of L_i, while $\boldsymbol{\eta}_i^\perp$ is the direction perpendicular to $\boldsymbol{P}_i$, which is, therefore, tangent to L_i. From this construction, it follows that Bragg lines on $\partial\Omega$ must come in pairs. In particular, if $\boldsymbol{P}$ is a neighbor of $\mathbf{0}$ and the Bragg line crossing $\boldsymbol{P}/2$ lies on $\partial\Omega$, it follows by symmetry that the Bragg line crossing $-\boldsymbol{P}/2$ must also lie on $\partial\Omega$.

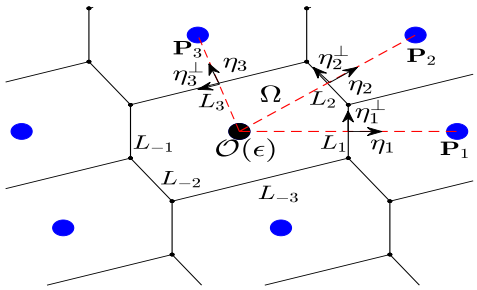

Figure 9: Schematic of the detailed construction of the FWS cell showing the three pairs of parallel Bragg lines for the specific oblique lattice in Fig. 1. The trap (black circle) of measure $\mathcal{O}(\varepsilon)$ is centered at the origin.

Next, we reformulate the PDE (3.6) for the periodic Helmholtz Green's function G_λ on $\mathbb{R}^2$ to an equivalent PDE on the FWS cell. This is done by imposing a boundary operator $\mathcal{P}$ on $\partial\Omega$ that incorporates the periodic condition in (3.6). This equivalent PDE is

$$\Delta G_\lambda + \lambda_{0s} G_\lambda = -\delta(\boldsymbol{x})\,, \quad \boldsymbol{x}\in\Omega\,; \qquad G_\lambda \in \mathcal{P}\,, \quad \boldsymbol{x}\in\partial\Omega\,; \qquad R_\lambda \equiv \lim_{\boldsymbol{x}\to\mathbf{0}}\left(G_\lambda(\boldsymbol{x}) + \frac{1}{2\pi}\log|\boldsymbol{x}|\right). \tag{A.6}$$

In (A.6), the boundary operator is defined by

$$\mathcal{P} \equiv \left\{ u \,\middle|\, \begin{pmatrix} u(\boldsymbol{x}_{i1}) \\ \partial_n u(\boldsymbol{x}_{i1}) \end{pmatrix} = \begin{pmatrix} u(\boldsymbol{x}_{i2}) \\ \partial_n u(\boldsymbol{x}_{i2}) \end{pmatrix}, \quad \forall\, \boldsymbol{x}_{i1}\in L_i\,, \ \forall\, \boldsymbol{x}_{i2}\in L_{-i}\,, \quad i=1,\ldots,L/2 \right\}. \tag{A.7}$$

Here L_i and L_{-i} denote two parallel Bragg lines on opposite sides of $\partial\Omega$ for $i=1,\ldots,L/2$, while $\boldsymbol{x}_{i1}\in L_i$ and $\boldsymbol{x}_{i2}\in L_{-i}$ are any two opposing points on these Bragg lines. A schematic plot of the FWS cell showing the pairs of Bragg lines for the particular oblique lattice of Fig. 1 is given in Fig. 9.

B The periodic Helmholtz Green's function

In this appendix we outline the approach used in [2] for deriving (3.8). We begin by representing the solution to (3.6) as the sum of free-space Green's functions

$$G_\lambda(\boldsymbol{x}) = \sum_{\boldsymbol{l}\in\Lambda} G_{\text{free}}(\boldsymbol{x}+\boldsymbol{l})\,, \tag{B.1}$$

which ensures that the periodicity condition in (3.6) is satisfied. Then, to analyze (B.1) we use the Poisson summation formula which converts a sum over the Bravais lattice Λ to a sum over the reciprocal lattice $\Lambda^\star$ of (3.9). In the notation of [2], we have that this summation formula is given by (see Proposition 2.1 of [2])

$$\sum_{\boldsymbol{l}\in\Lambda} f(\boldsymbol{x}+\boldsymbol{l}) = \frac{1}{|\Omega|}\sum_{\boldsymbol{d}\in\Lambda^\star} \hat{f}(2\pi\boldsymbol{d})\, e^{2\pi i \boldsymbol{x}\cdot\boldsymbol{d}}\,, \qquad \boldsymbol{x}\in\mathbb{R}^2\,. \tag{B.2}$$

Here $|\Omega|$ is the area of the primitive cell of the lattice, while $\hat{f}$ is the Fourier transform of f, defined on $\mathbb{R}^2$ by

$$\hat{f}(\boldsymbol{p}) \equiv \int_{\mathbb{R}^2} f(\boldsymbol{x})\, e^{-i\boldsymbol{x}\cdot\boldsymbol{p}}\, \mathrm{d}\boldsymbol{x}\,, \qquad f(\boldsymbol{x}) = \frac{1}{4\pi^2}\int_{\mathbb{R}^2} \hat{f}(\boldsymbol{p})\, e^{i\boldsymbol{p}\cdot\boldsymbol{x}}\, \mathrm{d}\boldsymbol{p}\,. \tag{B.3}$$

Upon applying (B.2) to (B.1) we obtain that the sum over the reciprocal lattice consists of free-space Green's functions in the Fourier domain. By taking the Fourier transform of the PDE $\Delta G_{\text{free}} + \lambda_{0s} G_{\text{free}} = -\delta(\boldsymbol{x})$ for the free-space Green's function, we obtain that $\hat{G}_{\text{free}}(\boldsymbol{p}) = \hat{G}_{\text{free}}(|\boldsymbol{p}|)$, where

$$\hat{G}_{\text{free}}(\rho) = \frac{1}{\rho^2 - \lambda_{0s}}\,, \qquad \text{with} \quad \rho \equiv |\boldsymbol{p}|\,, \tag{B.4}$$

for $\rho^2 \neq \lambda_{0s}$. Then, from (B.2) and (B.1), and by using $|\Omega| = 1$, we obtain that

$$G_\lambda(\boldsymbol{x}) = \frac{1}{|\Omega|}\sum_{\boldsymbol{d}\in\Lambda^\star} \hat{G}_{\text{free}}(2\pi\boldsymbol{d})\, e^{2\pi i\boldsymbol{x}\cdot\boldsymbol{d}} = \sum_{\boldsymbol{d}\in\Lambda^\star} \frac{e^{2\pi i\boldsymbol{x}\cdot\boldsymbol{d}}}{4\pi^2|\boldsymbol{d}|^2 - \lambda_{0s}}\,. \tag{B.5}$$

In order to obtain a rapidly converging infinite series representation for $G_\lambda(\boldsymbol{x})$, we introduce the decomposition

$$\hat{G}_{\text{free}}(2\pi\boldsymbol{d}) = \alpha(2\pi\boldsymbol{d},\eta)\,\hat{G}_{\text{free}}(2\pi\boldsymbol{d}) + \Big(1 - \alpha(2\pi\boldsymbol{d},\eta)\Big)\,\hat{G}_{\text{free}}(2\pi\boldsymbol{d})\,, \tag{B.6}$$

where the function $\alpha(2\pi\boldsymbol{d},\eta)$ is defined by

$$\alpha(2\pi\boldsymbol{d},\eta) = \exp\left(-\frac{\big[4\pi^2|\boldsymbol{d}|^2 - \lambda_{0s}\big]}{\eta^2}\right)\,. \tag{B.7}$$

Here $\eta > 0$ is a real-valued cutoff parameter. When $4\pi^2|\boldsymbol{d}|^2 > \lambda_{0s}$ we readily calculate that

$$\lim_{\eta\to 0}\alpha(2\pi\boldsymbol{d},\eta) = 0\,; \qquad \lim_{\eta\to\infty}\alpha(2\pi\boldsymbol{d},\eta) = 1\,.$$

With this choice for α, the sum over $\boldsymbol{d}\in\Lambda^\star$ in (B.5) of the first set of terms in (B.6), as labeled by

$$G_{\text{fourier}}(\boldsymbol{x}) \equiv \sum_{\boldsymbol{d}\in\Lambda^\star} \exp\left(-\frac{\big[4\pi^2|\boldsymbol{d}|^2 - \lambda_{0s}\big]}{\eta^2}\right)\,\frac{e^{2\pi i\boldsymbol{x}\cdot\boldsymbol{d}}}{4\pi^2|\boldsymbol{d}|^2 - \lambda_{0s}}\,, \tag{B.8}$$

converges absolutely when $\lambda_{0s} \neq 4\pi^2|\boldsymbol{d}|^2$ for any $\boldsymbol{d}\in\Lambda^\star$.

Next, we calculate the lattice sum in (B.5) over the second set of terms in (B.6) by using the inverse transform (B.3) after first writing $(1-\alpha)\,\hat{G}_{\text{free}}$ as an integral. To do so, we define $\rho \equiv 2\pi|\boldsymbol{d}|$, so that from (B.7) and (B.4)

$$\big(1 - \alpha(2\pi\boldsymbol{d},\eta)\big)\,\hat{G}_{\text{free}}(2\pi\boldsymbol{d}) = \frac{1}{\rho^2-\lambda_{0s}}\left(1 - \exp\left(-\frac{\big[\rho^2-\lambda_{0s}\big]}{\eta^2}\right)\right) = \hat{\chi}(\rho) \equiv \int_{\log\eta}^{\infty} 2\, e^{-\left(\rho^2-\lambda_{0s}\right)e^{-2s} - 2s}\, ds\,. \tag{B.9}$$

In recognizing the middle term in (B.9) as the integral $\hat{\chi}(\rho)$ we used the easily verified definite integral

$$2\int_{\log\eta}^{\infty} e^{-\left(\rho^2-\lambda_{0s}\right)e^{-2s} - 2s}\, ds = \frac{e^{-\left(\rho^2-\lambda_{0s}\right)e^{-2s}}}{\rho^2-\lambda_{0s}}\bigg|_{s=\log\eta}^{s=\infty} = \frac{1}{\rho^2-\lambda_{0s}}\left(1 - \exp\left(-\frac{\big[\rho^2-\lambda_{0s}\big]}{\eta^2}\right)\right)\,. \tag{B.10}$$

Next, we take the inverse Fourier transform of (B.9). To do so, we use two key facts. Firstly, the inverse Fourier transform of a radially symmetric function $\hat{f}(\rho)$ is the inverse Hankel transform of order zero (cf. [25]), so that $f(r) = (2\pi)^{-1}\int_0^\infty \hat{f}(\rho)\, J_0(\rho r)\,\rho\, d\rho$. Secondly, from [25], we recall the well-known inverse Hankel transform

$$\int_0^\infty e^{-\rho^2\, e^{-2s}}\,\rho\, J_0(\rho r)\, d\rho = \frac{1}{2}\, e^{2s - r^2\, e^{2s}/4}\,.$$

In this way, we calculate using the definition of $\hat{\chi}(\rho)$ in (B.9) that

$$\chi(r) \equiv \frac{1}{2\pi}\int_0^\infty \hat{\chi}(\rho)\, J_0(\rho r)\, \rho\, d\rho = \frac{1}{\pi}\int_{\log\eta}^\infty e^{-2s+\lambda_{0s}e^{-2s}} \left(\int_0^\infty e^{-\rho^2 e^{-2s}}\, \rho\, J_0(\rho r)\, d\rho\right) ds$$
$$= \frac{1}{2\pi}\int_{\log\eta}^\infty e^{-2s+\lambda_{0s}e^{-2s}}\, e^{2s-\frac{r^2}{4}e^{2s}}\, ds = \frac{1}{2\pi}\int_{\log\eta}^\infty e^{-\left(\frac{r^2}{4}e^{2s}-\lambda_{0s}\,e^{-2s}\right)}\, ds\,.$$

In the notation of [2], we then define $F_{\rm sing}(|\boldsymbol{x}|)$ as

$$F_{\rm sing}(|\boldsymbol{x}|) \equiv \frac{1}{2\pi}\int_{\log\eta}^\infty e^{-\left(\frac{|\boldsymbol{x}|^2}{4}e^{2s}-\lambda_{0s}\,e^{-2s}\right)}\, ds\,. \tag{B.11}$$

Therefore, by using the Poisson summation formula (B.2) to calculate lattice sum in (B.5) over the second set of terms in (B.6), we obtain

$$G_{\rm spatial}(\boldsymbol{x}) \equiv F_{\rm sing}(|\boldsymbol{x}|) + \sum_{\substack{\boldsymbol{l}\in\Lambda\\ \boldsymbol{l}\neq\boldsymbol{0}}} F_{\rm sing}(|\boldsymbol{x}+\boldsymbol{l}|)\,. \tag{B.12}$$

In summary, the periodic Helmholtz Green's function in the spatial domain, satisfying (3.6), is $G_\lambda(\boldsymbol{x}) = G_{\rm fourier}(\boldsymbol{x}) + G_{\rm spatial}(\boldsymbol{x})$, representing the sum of (B.8) and (B.12). In this way, we obtain the result given in (3.8). In terms of the Ewald cut-off parameter η, we observe from (B.8) that $G_{\rm fourier}(\boldsymbol{x}) \to 0$ as $\eta \to 0$, while from (B.12) and (B.11) we get that $G_{\rm spatial}(\boldsymbol{x}) \to 0$ as $\eta \to \infty$.

C An alternative derivation for $F_{\rm sing}(r)$ and its singular behavior

In this appendix we provide an alternative derivation of the singular behavior for $F_{\rm sing}(r)$ in (3.19) as $r \to 0$. We begin by balancing the two terms in the exponential in (3.8b) by defining s_m by $r^2 e^{2s_m}/4 = \lambda_{0s} e^{-2s_m}$. Then, in (3.8b), we introduce the new variable t defined by

$$s = s_m + \frac{t}{2}\,, \qquad \text{where} \qquad s_m = \frac{1}{4}\log\left(\frac{4\lambda_{0s}}{r^2}\right)\,, \tag{C.1}$$

so that (3.8b) becomes

$$F_{\rm sing}(r) = \frac{1}{4\pi}\int_\beta^\infty e^{-r\sqrt{\lambda_{0s}}\sinh t}\, dt\,, \qquad \text{where} \qquad \beta \equiv \log\left(\frac{\eta^2 r}{2\sqrt{\lambda_{0s}}}\right)\,. \tag{C.2}$$

Next, we recall Schläffi's representation for the Bessel function of the second kind of order zero, $Y_0(x)$, as given for $x > 0$ by (cf. [23])

$$Y_0(x) = \frac{1}{\pi}\int_0^\pi \sin\left(x\sin t\right)\, dt - \frac{2}{\pi}\int_0^\infty e^{-x\sinh t}\, dt\,. \tag{C.3}$$

Setting $x = \sqrt{\lambda_{0s}}r$ in (C.3), we use (C.3) to write (C.2) as

$$F_{\rm sing}(r) = -\frac{1}{8}Y_0\left(r\sqrt{\lambda_{0s}}\right) + \frac{1}{8\pi}\int_0^\pi \sin\left(r\sqrt{\lambda_{0s}}\sin t\right)\, dt + J\,, \qquad \text{where} \qquad J \equiv \frac{1}{4\pi}\int_\beta^0 e^{-r\sqrt{\lambda_{0s}}\sinh t}\, dt\,. \tag{C.4}$$

Next, since $\beta \to -\infty$ as $r \to 0^+$, while $\sinh t \to -\infty$ as $t \to -\infty$, it follows that J is unbounded as $r \to 0$. To analyze the singular behavior of J, we introduce the new variable s by $s = \sinh t/\sinh\beta$ in the integrand to obtain that

$$F_{\rm sing}(r) = -\frac{1}{8}Y_0\left(r\sqrt{\lambda_{0s}}\right) + \frac{1}{8\pi}\int_0^\pi \sin\left(r\sqrt{\lambda_{0s}}\sin t\right)\, dt + J\,, \quad \text{where} \quad J \equiv -\frac{\text{sign}(\beta)}{4\pi}\int_0^1 \frac{e^{-rs\sqrt{\lambda_{0s}}\sinh\beta}}{\sqrt{s^2+\text{csch}^2\beta}}\, ds\,. \tag{C.5}$$

Next, we use (C.2) for β to calculate

$$\sinh\beta = -\frac{\sqrt{\lambda_{0s}}}{\eta^2 r} + \frac{\eta^2 r}{4\sqrt{\lambda_{0s}}} \sim -\frac{\sqrt{\lambda_{0s}}}{\eta^2 r} \quad \text{as} \quad r \to 0^+ \,. \tag{C.6}$$

In this way, and by using $\text{sign}(\beta) = -1$, we obtain for $r \ll 1$ that

$$J \sim \frac{1}{4\pi}\int_0^1 \frac{e^{s\lambda_{0s}/\eta^2}}{\sqrt{s^2+\mu^2}}\, ds\,, \qquad \text{where} \qquad \mu \equiv \frac{r\eta^2}{\sqrt{\lambda_{0s}}}\,. \tag{C.7}$$

We then add and subtract a term in (C.7) as

$$J \sim \frac{1}{4\pi}\int_0^1 \frac{\left(e^{s\lambda_{0s}/\eta^2}-1\right)}{\sqrt{s^2+\mu^2}}\, ds + \frac{1}{4\pi}\int_0^1 \frac{1}{\sqrt{s^2+\mu^2}}\, ds\,, \tag{C.8}$$

so that the first integral is now convergent as $\mu \to 0$, corresponding to $r \to 0^+$. Moreover, the second integral in (C.8) can be evaluated explicitly. This yields that

$$\begin{aligned} J &\sim \frac{1}{4\pi}\int_0^1 \frac{\left(e^{s\lambda_{0s}/\eta^2}-1\right)}{s}\, ds + \frac{1}{4\pi}\log\left(\sqrt{1+\frac{s^2}{\mu^2}}+\frac{s}{\mu}\right)\Big|_0^1\,, \\ &\sim \frac{1}{4\pi}\int_0^1 \frac{\left(e^{s\lambda_{0s}/\eta^2}-1\right)}{s}\, ds - \frac{1}{4\pi}\log\mu + \frac{1}{4\pi}\log\left(1+\sqrt{1+\mu^2}\right)\,. \end{aligned} \tag{C.9}$$

By using $\mu = r\eta^2/\sqrt{\lambda_{0s}}$ in the last line of (C.9), and by changing variables in the integral, we conclude that

$$J = \frac{1}{4\pi}\int_0^{\lambda_{0s}/\eta^2} \frac{(e^s-1)}{s}\, ds - \frac{1}{4\pi}\log r + \frac{1}{4\pi}\left[\log(\sqrt{\lambda_{0s}}) - 2\log\eta + \log 2\right] + o(1)\,, \quad \text{as} \quad r \to 0^+\,. \tag{C.10}$$

Then, we let $r \to 0$ in (C.5) while using (C.10) together with the well-known asymptotics $Y_0(z) \sim \frac{2}{\pi}\left[\log z + \gamma_e - \log 2\right]$ as $z \to 0^+$ and $\int_0^\pi \sin\left(\sqrt{\lambda_{0s}} r \sin t\right)\, dt = \mathcal{O}(r)$ as $r \to 0$. This yields that $F_{\text{sing}}(r) = -(2\pi)^{-1}\log r + F_{\text{reg}} + o(1)$ as $r \to 0$, where

$$F_{\text{reg}} = \frac{1}{4\pi}\left(\log 4 - \gamma_e - 2\log\eta\right) + \frac{1}{4\pi}\int_0^{\lambda_{0s}/\eta^2} \frac{(e^s-1)}{s}\, ds\,. \tag{C.11}$$

This result for F_{reg} agrees with that in (3.11b), while the exact result for $F_{\text{sing}}(r)$ in (C.5) provides an alternative to that in (3.11c).

References

[1] M. Aguarles and J. de Haro. Derivation of the maximum voltage drop in power grids of integrated circuits with an array bonding package. *Europ. J. Appl. Math.*, 23(6):787–819, 2012.

[2] G. Beylkin, C. Kurcz, and L. Monzón. Fast algorithms for Helmholtz Green's functions. *Proc. R. Soc. A*, 464:3301–3326, 2008.

[3] P. C. Bressloff. Asymptotic analysis of extended two-dimensional narrow capture problems, 2020. submitted to Proc. Roy. Soc. A.

[4] T. Carroll and Ortega-Cerdà J. The maximum voltage drop in an on-chip power distribution network: Analysis of square, triangular, and hexagonal power pad arrangements. *Europ. J. Appl. Math.*, 25(5):531–551, 2014.

[5] S. J. Chapman, D. P. Hewett, and L. N. Trefethen. Mathematics of the Faraday cage. *SIAM Review*, 57(3):398–417, 2015.

[6] X. Chen and Y. Oshita. An application of the modular function in nonlocal variational problems. *Arch. Rat. Mech. Anal.*, 186(1):109–132, 2007.

[7] D. A. Coker and S. Torquato. Simulation of diffusion and trapping in digitized heterogeneous media. *J. Appl. Phys.*, 77:955, 1995.

[8] W. Dijkstra and M. E. Hochstenbach. Numerical approximation of the logarithmic capacity, 2008. CASA Report 08-09, Technical U. Eindhoven.

[9] FlexPDE. *PDE Solutions inc*, 2015. Available at http://www.pdesolutions.com.

[10] D. Grebenkov. Spectral theory of imperfect diffusion-controlled reactions on heterogeneous catalytic surfaces. *J. Chem. Phys.*, 151:104108, 2019.

[11] J. Hinch. *Perturbation Methods*. Cambridge Texts in Applied Mathematics. Cambridge University Press, Cambridge, U.K., 1991.

[12] D. Iron, J. Rumsey, M. J. Ward, and J. C. Wei. Logarithmic expansions and the stability of periodic patterns of localized spots for reaction-diffusion systems in $\mathbb{R}^2$. *J. Nonlin. Science*, 24(5):564–627, 2014.

[13] S. Iyaniwura, J. Gou, and M. J. Ward. Synchronous oscillations for a coupled cell-bulk pde-ode model with localized cells on $\mathbb{R}^2$, 2021. to appear, J. Eng. Math. (24 pages).

[14] S. Iyaniwura and M. J. Ward. Asymptotic analysis for the mean first passage time in finite or spatially periodic 2-D domains with a cluster of small traps, 2021. to appear, ANZIAM J. (25 pages).

[15] S. Iyaniwura, T. Wong, C. B. MacDonald, and M. J. Ward. Optimization of the mean first passage time in near-disk and elliptical domains in 2-d with small absorbing traps, 2020. submitted to SIAM Review.

[16] A. R. Kansal and S. Torquato. Prediction of trapping rates in mixtures of partially absorbing spheres. *J. Chem. Phys.*, 116(24), 2002.

[17] T. Kolokolnikov, M. S Titcombe, and M. J Ward. Optimizing the fundamental Neumann eigenvalue for the Laplacian in a domain with small traps. *European Journal of Applied Mathematics*, 16(2):161–200, 2005.

[18] M. C. Kropinski, A. Lindsay, and M. J Ward. Asymptotic analysis of localized solutions to some linear and nonlinear biharmonic eigenvalue problems. *Studies in Applied Math*, 126(4):397–408, 2011.

[19] V. Kurella, J. C Tzou, D. Coombs, and M. J Ward. Asymptotic analysis of first passage time problems inspired by ecology. *Bulletin of Mathematical Biology*, 77(1):83–125, 2015.

[20] A. Lindsay, T. Kolokolnikov, and M. J Ward. The transition to point constraint in a mixed biharmonic eigenvalue problem. *SIAM J. Appl. Math.*, 75(3):1193–1224, 2015.

[21] A. E. Lindsay, J. C. Tzou, and T. Kolokolnikov. Narrow escape problem with mixed trap and the effect of orientation. *Phys. Rev. E.*, 91(3):032111, 2015.

[22] The Mathworks, Inc., Natick, Massachusetts. *MATLAB version 9.4.0.813654 (R2018a)*, 2018.

[23] F. W. J. Olver, A. B. O. Daalhuis, D. W. Lozier, B. I. Schneider, R. F. Boisvert, C. W. Clark, B. R. Miller, B. V. Saunders, H. S. Cohl, and M. A. (Eds.) McClain, 2012. NIST Digital Library of Mathematical Functions. Release 1.0.26 of 2020-03-15. Available online: http://dlmf.nist.gov/.

[24] S. Ozawa. Singular variation of domains and eigenvalues of the Laplacian. *Duke Math. J.*, 48(4):767–778, 1981.

[25] R. Piessens. The Hankel transform. In A. D. Poularikas, editor, *Transforms and Applications Handbook*, chapter 9. CRC Press, Boca Raton, Florida, 3rd edition, 2018.

[26] S. Pillay, M. J Ward, A Peirce, and T. Kolokolnikov. An asymptotic analysis of the mean first passage time for narrow escape problems: Part i: Two-dimensional domains. *SIAM J. Multiscale Model. Simul.*, 8(3):803–835, 2010.

[27] T. Ransford. *Potential theory in the complex plane*. London Math. Soc. Stud. Texts 28. Cambridge University Press, Cambridge, U.K., 1995.

[28] J. Sanchez Hubert and E. Sanchez Palencia. *Vibration and coupling of continuous systems*. Springer, Berlin, Heidelberg, 1989.

[29] O. Schnitzer and R. V. Craster. Bloch waves in an arbitrary two-dimensional lattice of subwavelength Dirichlet scatterers. *SIAM J. Appl. Math.*, 77(6):2119–2135, 2017.

[30] D. C. Torney and B. Goldstein. Rates of diffusion-limited reaction in periodic systems. *J. Stat. Phys.*, 49:725–750, 1987.

[31] N. Trefethon. Series solution of Laplace problems. *ANZIAM J.*, 60:1–26, 2018.

[32] J. C Tzou and T. Kolokolnikov. Mean first passage time for a small rotating trap inside a reflective disk. *SIAM J. Multiscale Model. Simul.*, 13(1):231–255, 2015.

[33] M. J Ward. Spots, traps, and patches: Asymptotic analysis of localized solutions to some linear and nonlinear diffusive systems. *Nonlinearity*, 31(8):R189, 2018.

[34] M. J. Ward, W. D. Henshaw, and J. B. Keller. Summing logarithmic expansions for singularly perturbed eigenvalue problems. *SIAM J. Appl. Math.*, 53(3):799–828, 1993.

[35] M. J Ward and J. B Keller. Strong localized perturbations of eigenvalue problems. *SIAM J. Appl. Math.*, 53(3):770–798, 1993.